Optimization of Tooth-root Profile for Maximum Load-carrying Capacity: Spur and Bevel Gears

Mathew Shaker

Master of Engineering

Mechanical Engineering

McGill University

Montreal,Quebec

2014-12-15

A thesis submitted to the Faculty of Graduate Studies and Research
in partial fulfillment of the requirements for the degree of
Master of Engineering

ACKNOWLEDGEMENTS

First and foremost, I would like to express my deepest gratitude to my supervisor, Professor Jorge Angeles, for his continuous guidance, support and patience during the course of my graduate studies at McGill University. His vast knowledge and experience in engineering has set the path for me to complete this research.

I would also like to thank Dr. Ting Zou for her great assistance and valuable advice with regards to Finite Element Analysis and also technical report writing. I want to thank Dr. Alexei Morozov and my colleague Guillaume Sauze for all the valuable discussions in our weekly meetings.

The Centre for Intelligent Machines (CIM) of McGill University has provided the resources and the means to conduct this research. I would like to thank the administrative officers for all their hard work in always meeting our needs.

The support of the Automotive Partnership Canada (APC) grant APCPJ418901-11 is also highly acknowledged. Thanks to all the academic and industrial staff involved in this project for all the interdisciplinary discussions and fruitful meetings.

ABSTRACT

Increasing the strength of the gear tooth is a recurrent demand from industry. In this thesis a novel approach to the design of the tooth-root profile of spur and bevel gears using non-parametric cubic splines, with the aim of increasing the gear strength, is introduced. Bevel gears generated using the Tredgold approximation and the exact spherical involute were considered. The shape of the root profile was smoothed so as to endow it with G^2-continuity, thereby reducing the stress concentration at the critical blending points. An iterative co-simulation procedure consisting of tooth-root profile shape synthesis via non-linear programming and finite element analysis was conducted. The proposed designs are capable of reducing the stress concentration by 20.0% in spur gears, 15.9% and 19.3% in the Tredgold approximation and the exact spherical involute bevel gears, respectively.

ABRÉGÉ

Augmenter la résistance des dents d'engrenages est une éxigeance récurrente dans les industries. Dans cette thèse, une nouvelle approche à la conception de la racine des profils de dents des engrenages planaires et coniques, en utilisant des courbes spline cubiques non-paramétriques, afin d'augmenter la résistance des engrenages, est proposée. Des engrenages coniques, générés en utilisant l'approximation de Tredgold ou le profil à développante sphérique exacte, ont été étudiés. La forme du profil de la racine de la dent est assouplie de telle sorte à ajouter une continuité de classe G^2, ainsi réduisant la concentration des contraintes aux points critiques. Une procédure itérative de co-simulation consistant en la synthèse de la racine des profils de dents, par programmation non-linéaire et analyse par éléments finis, fut mise en place. Les conceptions ainsi proposées permirent de réduire la concentration des contraintes de 20% pour les engrenages planaires, ainsi que, respectivement, 15.9% et 19.3% dans le cas de l'utilisation de l'approximation de Tredgold et dans le cas du profil à développante sphérique exacte, pour des engrenages coniques.

TABLE OF CONTENTS

LIST OF TABLES

LIST OF FIGURES

CHAPTER 1
Introduction

1.1 Background and Motivation

Gears are mechanical components used to transmit power and motion through the successive engagement of their peripheral teeth. They perform multiple functions in mechanical systems and machines, including altering speed ratios, reversing the rotation direction, changing the angular orientation of rotary motion and converting rotary motion into translation and vice versa. The gear is a key component in transmission systems; therefore, its reliability and stability is essential to meet the performance requirements of the system. Gear teeth that break become debris that can cause a complete machine breakdown in a very short time. This can be extremely dangerous, especially in applications such as automotive gear systems. A growing demand for gears with higher load-carrying capacity and increased fatigue life accompanies the fast development of automotive transmissions. There are several ways to achieve that, namely using new materials, improved heat-treatment or novel gear geometries [2].

The gear tooth is exposed to a combination of several effects under working conditions, such as stress concentration, misalignment, tooth error, etc. [3]. When transmitting loads, each gear tooth behaves as a cantilever beam, subjected to bending [4]. The maximum bending stress of the gear tooth evolves from the accumulation of normal stress under bending and appears at the root fillet. The gear tooth-root is exposed to a combination of both shearing and bending [5]. Repeated excessive stresses cause bending fatigue often at the tooth-root [2]. The first crack initiates at the regions with the highest stress concentrations and propagates until failure occurs [6]. Within the development history of gear design, the fatigue of gear tooth due to bending is always a challenge to designers.

Conventional gears are designed with a circular-filleted tooth-root [2]. A circular fillet avoids stress concentrations that would arise due to an infinite curvature at the corner between the tooth flank and the root circle. However, at the blending points of the circular fillet with the involute tooth profile and the root circle, stress concentration occurs due to curvature discontinuity. Such discontinuities cause a drastic jump in stress values, thereby making these regions prone to mechanical failure. Hence, the optimization of the gear tooth-root profile plays a significant role in reducing the stress concentration and improving the gear tooth strength.

In this work, an innovative optimization procedure combining shape synthesis via nonlinear programming and FEA software package tools is developed to produce the tooth-root fillet for spur and bevel gears with minimum stress concentration. The *Tredgold approximation* (TA) and the *exact spherical involute* (ESI) tooth profile for bevel gears were considered [7]. The FEA results show a significant reduction in the maximum von Mises stress of the optimum tooth profile when compared with its circular counterpart.

1.2 History and Applications of Gears

The Chinese south-pointing chariot shown in Fig. 1–1 is one of the oldest geared mechanisms. The date of this device ranges back to the 27th century B.C. It consists of a statue with a pointing arm on top of a chariot. The function of the statue is to point in the same direction regardless of the route followed by the chariot, thereby acting as a mechanical compass. The wheels were mechanically geared to keep the statue always pointing in the same direction.

Figure 1–1: The Chinese south-pointing chariot

Heron of Alexandria, a native of Roman Egypt, was a Greek mathematician who invented many geared mechanisms. That included the water dispenser which was coin-operated and the temple gate opener. Leonardo Da Vinci devised many mechanisms that employed gears. One of his famous machines is the lens-grinding machine which had an angle-gear and a geared dish.

In the 18th century, Leonhard Euler proposed the use of the involute of a circle as the profile of gear teeth (involute gear), a remarkable design which is still used today. In the 19th century form-cutters were introduced. The first hobbing machine was invented by the German Hermann Pfauter in 1897.

Until today, gears are extensively used as the building blocks of many mechanical drives, which transfer mechanical power from the prime mover to the actuator [1]. Depending on the application, the mechanical drive is necessary to link a machine member and an actuator that should rotate at different speeds, or to actuate several actuators by using one prime mover, or to control the speed of an actuator without changing the machine speed. While some mechanical drives or transmissions use friction to transmit power, by means of friction wheels or belt drives, we focus on geared transmissions that employ toothed gears. Gear transmissions are seen in many applications and numerous industries.

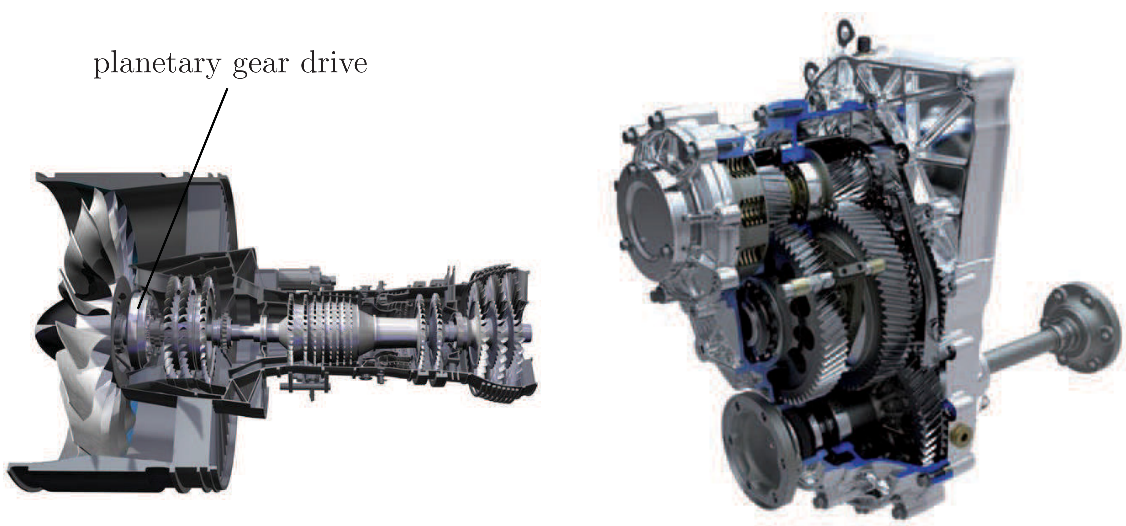

(a) P&W geared turbofan

(b) Œrlikon two-speed electric gearbox

Figure 1–2: Gear applications

In the aerospace and automotive industry, gear drives continue to be extensively used. New geared turbofan engines are currently being produced by Pratt & Whitney (P&W). The engine makes use of a planetary gear train as shown in Fig. 1–2a to run a bigger fan at lower speeds. As a result, the engine fan can be operated at subsonic rather than supersonic speeds, hence reducing noise and improving efficiency. Multi-speed drive trains are now being developed for fully electric vehicles to increase efficiency, vehicle speed and driving range without drawing additional battery power. Fig. 1–2b shows a double stage reduction gearbox manufactured by Œrlikon Graziano for electric passenger cars or light commercial vehicles. The Automotive Partnership Canada project of Canada's National Sciences and Engineering Research Council (NSERC), currently targeting this market area to develop an optimal drivetrain for fully electric vehicles, has provided the funds for this research.

1.3 Review on Structural Optimization of Gears

Optimization problems in the early years were treated by classical techniques of differential calculus and calculus of variations. A small number of simple unconstrained or equality constrained problems were solved using these techniques obtaining exact solutions [8]. In the early 1960's, numerical approximation techniques were combined with mathematical programming methods for the first time to develop structural optimization algorithms [9].

The development of numerical approximation techniques, such as the Finite Element Method (FEM), Boundary Element Method (BEM) and Finite-difference Method (FDM), allowed the solving of problems too intricate to be solved by long-hand calculations [8]. The FEM in particular, named so by Clough in 1960 [10], became dominant in many engineering disciplines such as biomechanics, computational fluid dynamics and solid mechanics [11]. Since then computers have been used extensively in many industrial sectors, including the automotive and aerospace industry. In the area of mechanical design, the FEM is used to calculate stress and displacement magnitudes, which are used to assess device-performance. In the 1970s, Armand [12] and Gallagher [13] used numerical approximation techniques in structural optimization.

Establishing an optimality criterion was the next development. In 1971, Venkayya suggested an optimality criterion whereby the minimum-weight structure is the one in which the strain energy density is constant throughout the structure [14]. In 1976, Mroz and Garstecki worked on the optimal design of structural elements with unspecified load distribution [15].

As computer-aided design (CAD) systems gained popularity, geometric approaches to shape optimization evolved. That is, the design parameters in the optimization problem defined the shape of the component at prespecified locations. In 1975, Francavilla et al. characterized the optimal shape defined by a set of geometric design parameters upon minimizing the stress concentration factors [16]. In 1977 Oda conducted an iterative procedure in which a predefined fundamental shape is modified based on the stresses obtained by carrying out a finite element analysis in each iteration [17].

Coupling of the CAD system to structural optimization was the next development. Esping solved the minimum-weight design problem by resorting to a CAD approach [18]. By using a set of lines, he defined the members of a truss structure.

The values of the design variables were based on the position of the truss nodes and the objective function was formulated so as to minimize the truss weight. Parametric curves and CAD surfaces allowed the synthesis of complex shapes. Interest in the application of splines to curve synthesis was in continuous growth.

In 1983, Angeles showed how periodic splines can be used to synthesize curves that meet the local geometric properties of a finite set of points located through the interval of interest [19]. The curve-synthesis problem was of interest to designers in many technical areas. Determining the shape complying with certain geometric conditions such as prescribed values of slopes and/or curvature was a requirement in many problems such as synthesis of cam profiles, design of railroad tracks or conveyor belts etc. Existing methods at the time focused on the problem of interpolation given a set of interpolation points i.e., the interpolation points remained unchanged while the designer modified some of the parameters of the interpolation curve. In the approach proposed by Angeles, a method was introduced that determined a set of unknown interpolation points. The distribution of the local geometric properties that the approximating curve should have at the interpolation points was prescribed, then the curve was synthesized such that the prescribed values were met.

The curve synthesis concept using cubic splines presented by Angeles has been implemented in several structural optimization problems. Angeles et al. [20] published a two-level approach for the structural optimization of a spherical parallel manipulator. The proximal link thus designed belongs to a spherical mechanism called the Agile Wrist. The optimum design of the proximal link was obtained in two stages. In the first stage, the shape of the midcurve producing minimum stress concentrations was obtained by resorting to the concept of curve synthesis using cubic splines. Stress concentrations are induced by curvature discontinuities; hence, the requirements imposed on the midcurve were to blend as smoothly as possible at the blending points and to minimize curvature changes. The second stage involved obtaining the optimum cross-section along the midcurve producing a link of minimum weight. Several cross-sections were tested. The optimum solutions rendering the minimum weight link were generated. The scaling factors defining the size of the cross sections at several points along the midcurve were the design variables. The optimum solutions were then tested to determine which one renders minimum the volumetric strain energy. The approach resorted to FEA by using the optimization tool in the Structure module of Pro/Mechanica.

In 2012, a curve synthesis approach proposed by Angeles et al. [21] employs non-parametric cubic splines for the shape optimization of a self-deployable anchor designed for mitral valve repair. The anchor curve, which had to undergo high deformations was designed so as to minimize stress concentrations by enforcing curvature continuity. The von Mises stress in the optimum design was significantly reduced.

Structural optimization finds its applications in many mechanical parts. In this research we focus on gears. A gear is subjected to very high specific loads. The tooth-root is loaded by extremely high bending. If the bending stress at the tooth-root exceeds the material strength, a crack could initiate in the fillet, leading to a fatal failure [22]. In applications such as automotive transmissions, there is always a growing demand for gears with high bending strength and increased fatigue life.

Reducing bending stresses in gears is widely investigated in the literature with the aim of increasing the load-carrying capacity and extending the gear life. When reviewing the vast literature published, approaches in achieving the foregoing goal have been directed towards either identifying and selecting the optimum combination of gear geometrical parameters or optimizing the tooth-root fillet profile shape. The former was approached by Andrews and Hearn in 1987, who developed a design optimization procedure that modifies the tooth design parameters to reduce stress level in the root fillet while satisfying the functional constraints, that is, to maintain a practical design [23]. Design parameters included pressure angle, module, number of teeth and rack tip radius factor. The objective function was formulated to approximate the structural behaviour with respect to the design parameters. Finite Element Analysis was used to compute stress values in the fillet region. The optimization problem was solved using penalty-function methods, where the constrained problem is transformed to one of unconstrained optimization. Although the gear bending stress was reduced by having a larger pressure angle, undesirable effects were seen in the results, such as a lower contact ratio, which causes higher noise level and rough running of the gears. Thus, the gear load-carrying capacity in other types of failure modes such as pitting and scuffing, is reduced.

In 2002, Kapelevich et al. proposed an alternative method of design for spur and helical gears [24]. Since gear design is generally based on standard tools, the gears provided are usually not optimum. The author separated gear-geometry definition from tool selection; hence, the gear tooth profiles did not depend on the standard set of parameters of the generating rack and its location relative to a standard pitch diameter of the gear. The foregoing approach allowed gear designers to explore more gear combinations, which could provide better performance for a particular product or application. The next step is defining a unique tool geometry to generate the designed gear set; therefore, the cost of a custom cutting tool had to be added. Kapelevich has also developed involute gears with asymmetric tooth profiles for gear applications where opposite flanks of the gear tooth are functionally different.

Efforts to minimize fillet stresses by optimizing gear tooth geometry have been further reported by Spitas et al. [25]. Their approach uses nondimensional gear teeth in a stress minimization problem. The number of design variables is reduced by incorporating the geometrical parameters of the gear in the contact ratio of the pair, thus reducing computational time. The authors use boundary element analysis (BEA) to compute the maximum fillet stress. However, instead of modelling the gear tooth and running a BEA for every iteration,"stress tables" are used, which were precalculated by applying BEM on different combinations of the design parameters. By linear interpolation of the tabulated values, all the required intermediate values are readily calculated. The proposed optimum design was verified using two-dimensional photoelasticity. The procedure reports reduction in fillet stresses; however, it does not touch upon the fillet profile itself, which has a significant effect on the maximum stress value at the fillet region.

Volume and weight constraints are a major concern for designers and engineers in today's competitive automotive industry. Bian et al. introduced a multi-objective topology optimization approach for bevel gears [26]. The problem was formulated such that minimizing the weight of the bevel gear was the direct optimization goal while reducing contact stress, tooth root bending stress and improving flexibility. Bending stress and flexibility were set as design constraints by setting an upper bound for the former and a lower bound for the latter. A parameterized model of the bevel gear was created in CAD software. The tooth surface and the gear hole were fixed during the optimization process. The resulting gear structure had two through holes on each tooth and some small pits, thereby achieving a lighter design.

The gear tooth-root, an area of maximum tooth bending stress concentration, requires particular attention. Improving the geometry of the fillet results in substantial reduction in fillet stresses. Kapelevich et al. proposed a bending stress minimization technique based on curve fitting of the fillet profile to provide minimum bending stress concentration [27]. A random search method was used for the optimization problem where fillet nodes are moved along a prescribed path towards a common centre; the stress distribution is determined in every iteration. The initial fillet profile is a trajectory of the mating gear tooth tip. However, due to the random nature of the method, the results obtained were not always identical. Additionally, since continuity between fillet nodes cannot be guaranteed, wiggling shapes were often generated, which requires refinement to generate a smooth shape. The optimum fillet profile was approximated using trigonometric functions.

In 2005, Xiao et al. proposed a new shape-optimization approach which uses B-splines to represent the fillet shape [28]. The proposed method avoids the representation of the fillet profile by discrete nodes, which often leads to a huge number of design variables and does not guarantee continuity between elements. A genetic algorithm (GA) was taken as the optimizer. The control points of the B-splines were defined as design variables, as opposed to discrete nodes as in the former approach. Consequently, the number of design variables was reduced, as needed when using GA. A large number of design variables would often lead to an exponential increase in search-space dimension. The Boundary Element method (BEM) was used and an adaptive mesh generator was developed. While Xiao et al. resort to B-splines to synthesize the fillet profile, their procedure can be streamlined by curve synthesis using non-parametric cubic splines [29]. More importantly, the curve-synthesis problem can be formulated as an optimum design problem that can be solved using gradient methods, which are more robust than stochastic methods. Since a cubic spline passes through the control points, an adaptive mesh generator is not required, given that the node location is automatically selected to coincide with the control points, thereby guaranteeing a descent mesh distribution. An efficient technique for optimizing the tooth-root fillet shape will be demonstrated in this thesis.

Ristic analyzed the impact of the gear tooth fillet radius at the critical cross section on the stress values [30]. This work studied the effect of having two fillet radii in the tooth root region on the stress concentration. The second fillet radius acts as a "disencumber notch", which is supposed to lower the tooth root stress concentration. The spur gears considered were part of planetary transmission belonging to an excavator. By trial and error, the author conducted a series of iterations in which the radii of the fillets was varied systematically and a FEA was conducted to compute the maximum stress in the two fillet radii. The analysis showed that the proposed approach is not always correct as in many cases higher tooth root stresses were reported with two fillet radii rather than one. Increasing the radius of a circular fillet reduces the stress concentration because the curvature is minimized. However, there is a limit to the size of the fillet radius to avoid interference. Variation of the fillet stress with the tooth circular fillet radius is reported by Xie et al. [31]. The authors conducted a study on a helical gear that is part of an automotive transmission.

The multiple benefits of tooth fillet profile optimization leads to the topic of manufacturing with a concern on the how about of producing those customized fillets. Forming gear technology like powder metal processing, injection molding, extrusion etc. makes manufacturing of gear wheels with optimized tooth root fillet shapes possible. Flodin et al. talk about how powder metal manufacturing technology can be used to manufacture gears with optimized fillets in mass production [32]. It may be less efficient to use conventional methods of gear manufacturing in this case.

1.4 Thesis Contributions

The research work reported in this thesis focuses on a study of the load-carrying capacity of spur and bevel gears. Results of the study have been implemented on CAD models and tested using FEA. The major contributions are:

- Implementation of a curve synthesis approach to generate optimum gear tooth-root fillet profiles;
- formulating an innovative optimization procedure combining shape synthesis and FEA software tools to minimize stress concentrations in the tooth-root fillet;
- increasing the bending strength of spur gears, Tredgold-approximated and ESI bevel gears;

- achieving a more uniform stress distribution in the tooth-root region of spur and bevel gears.

CHAPTER 2
Geometric Modeling of Gears

2.1 Spur Involute Gears

Spur gears are used to transmit rotation between parallel shafts. Their teeth are cylindrical surfaces with generator parallel to the axis of rotation [33].

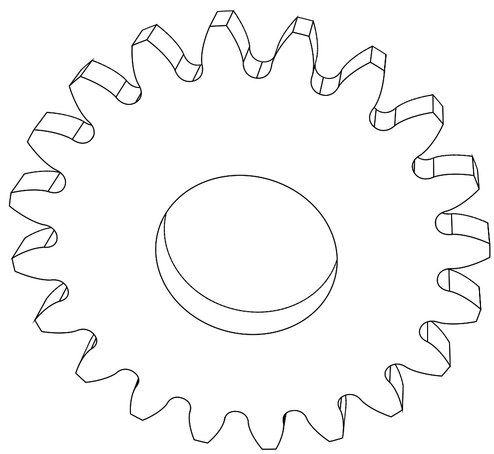

Figure 2–1: Spur gear model

Fig. 2–1 shows a spur gear model. The gear tooth profile has an involute shape. Involute gearing is widely used in industrial applications because of its numerous advantages. The transmission ratio of an involute gear is uniform and insensitive to small fluctuations in the centre distance. Transmission errors are therefore minimized and the gear operation is relatively silent. Involute cylindrical gears are also relatively simple to manufacture. The generation tools for involute gears can be produced with high precision. Additionally, involute gear tooth profiles can be readily varied using the same standard tools. The tooth thickness of involute gears can be changed providing nonstandard centre distances just by changing tool settings [34].

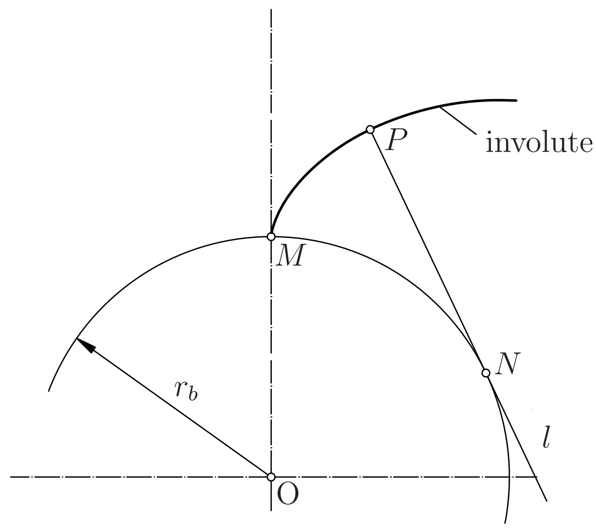

Figure 2–2: Involute of a circle

The involute of a circle is a roulette obtained by rolling of a straight line over the circle [1], as shown in Fig. 2–2. The circle, of radius r_b, is called the *base circle*. The generation of the involute of a circle can be demonstrated by imagining a cord as it wraps or unwraps around a circle. Any point on the unwrapped part of the cord traces out an involute. The involute has the following features:

- The normal at any point on the involute profile is tangent to the base circle.
- The radius of curvature of the involute at the point at which the normal is tangent to the base circle is $\rho = \overline{PN}$.

Figure 2–3 shows an illustration of an involute gear tooth. The involute profile shown is defined by

$$\begin{cases} x_{inv} = r_b(\cos t + t\sin t) \\ y_{inv} = r_b(\sin t - t\cos t) \end{cases}, \quad 0 \le t \le \sqrt{\frac{r_a^2}{r_b^2} - 1} \tag{2.1}$$

where the involute profile extends from the base circle to the *addendum circle*, of radius r_a.

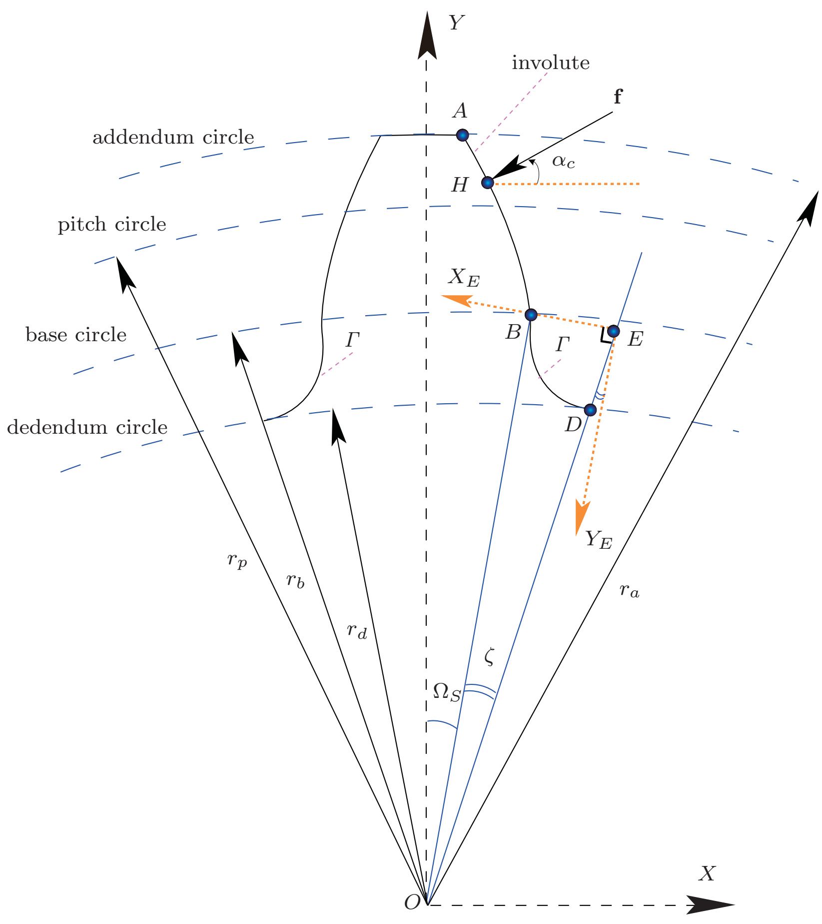

Figure 2–3: Geometry of the spur gear tooth

The reference circle for tooth element proportions is the *pitch circle*. The pitch circles of two gears in mesh are tangent to each other. The distance measured between two neighbouring teeth along the pitch circle is the *circular pitch* p. Hence,

$$p = \frac{\pi d}{N} \tag{2.2}$$

where d is the *pitch diameter* in mm and N is the *number of teeth*.

The *module* m is a scaling factor that is used as a measure of the circular pitch. It is given as

$$m = \frac{p}{\pi} = \frac{d}{N} \text{ mm} \tag{2.3}$$

The *addendum circle* of radius r_a lies on the top land of the tooth while the *dedendum circle* or *root circle* of radius r_d lies on the bottom land. The tooth-root fillet blends the end of the involute segment at the base circle with the dedendum circle.

Table 2–1: Dimensions of the spur gear model

number of teeth	20
module (mm)	24
face width (mm)	50
pressure angle (°)	20
addendum circle radius (mm)	264
pitch circle radius (mm)	240
base circle radius (mm)	225.526
dedendum circle radius (mm)	210

The *pressure angle* α_c is the angle between the transmitted force and the tangent to the wheel. The *face width* is the gear tooth length in the axial direction.

The dimensions of the spur gear model used in this research are given in Table 2–1.

2.2 Bevel Gears

Bevel gears transmit power between shafts intersecting at any angle. There are several types of bevel gears. Each type works best for a specific application, depending on the mountings, space available and operating conditions [1]. There are three types of bevel gears, depending on the tooth shape:

- Straight
- Helical
- Spiral

Straight bevel gears are widely used in automotive differentials. They are the simplest kind of bevel gears, having straight tapered teeth, as shown in Fig. 2–4.

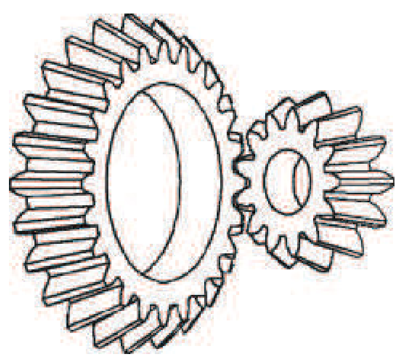

Figure 2–4: Straight bevel gears [1]

The basic parameters of straight bevel gears are shown in Fig. 2–5. The pitch diameter d_e of straight bevel gears is usually measured at the large end of the tooth, commonly called the *heel*. The small end of the tooth is called the *toe*. The circular pitch and module are calculated in the same manner as in the case of spur gears.

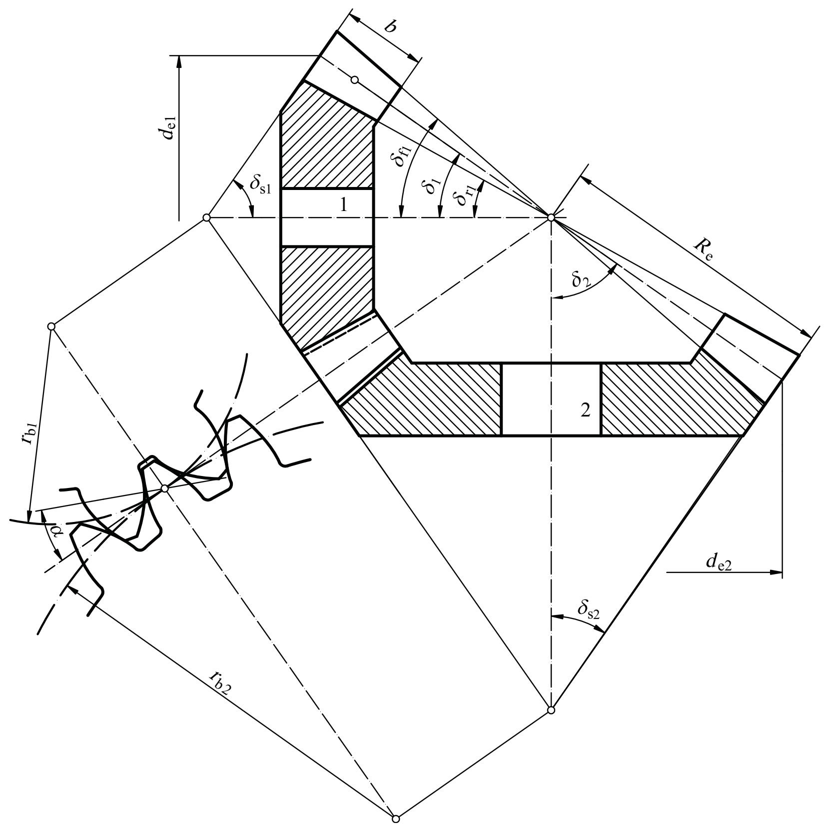

Figure 2–5: Straight bevel gear parameters

The pitch cones meet at the apex as shown in Fig. 2–5. The pitch cone angles of bevel gears 1 and 2 are δ_1 and δ_2, respectively. The pitch cone angles are related to the number of teeth by

$$\tan \delta_1 = \frac{N_2}{N_1} \quad \tan \delta_2 = \frac{N_1}{N_2} \tag{2.5}$$

The *face angle* and *root angle* of gear 1 are shown as δ_{1f} and δ_{1r}, respectively. The *back cone angle* is δ_s. The face width is b and the length of the outer cone is denoted as R_e.

The projection of a straight bevel gear onto a plane tangent to the back cone yields a *virtual* spur gear. Bevel gears designed based on the virtual spur gear lead to the TA [33]. The virtual spur gear has a pitch radius r_b equal to the back cone distance, as shown in Fig. 2–5. The number of teeth N' of the virtual spur gear is given by

$$N' = \frac{2\pi r_b}{p} \tag{2.6}$$

where p is the circular pitch measured at the heel.

A bevel gear set belonging to a differential manufactured by Linamar Corporation [1] is used in this research. The parameters of the bevel pinion and gear are given in Tables 2–2 and 2–3, respectively.

2.3 The Exact Spherical Involute

Commercial bevel gears have tooth profiles designed with either the Tredgold or the octoidal approximation, depending on the production machine used. Some are designed with the two approximations. The ESI profile was introduced to provide a uniform transmission ratio with a lower ripple effect than the TA. The design is

[1] An industrial partner of the Automotive Partnership Canada project at McGill University.

Table 2–2: Dimensions of bevel pinion

number of teeth	9
mating gear teeth	14
module (mm)	5.7658
pressure angle (°)	24
pitch angle (°)	32.735
face angle (°)	39.588
root angle (°)	24.530
face width (mm)	22.5
virtual gear number of teeth	11

Table 2–3: Dimensions of bevel gear

number of teeth	14
mating gear teeth	9
module (mm)	5.7658
pressure angle (°)	24
pitch angle (°)	57.265
face angle (°)	64.117
root angle (°)	49.059
face width (mm)	22.5
virtual gear number of teeth	26

insensitive to changes in shaft angles; therefore; the transmission ratio remains constant [35]. However, production methods for such tooth profiles are not commercially available; they are currently a subject area of research [36].

The ESI is the counterpart of the planar involute used in the production of spur gears. While the involute profile in the planar case was obtained by the rolling of a straight line on the base circle, in bevel gears it is obtained through the rolling motion of a great circle of the fundamental sphere on the base cone. The spherical involute is represented below in parametric form [37]:

$$x = \sin(\alpha \sin(\beta_b)) \cos(\alpha) - \sin(\alpha) \sin(\beta_b) \cos(\alpha \sin(\beta_b)) \quad (2.7)$$

$$y = -\sin(\alpha) \sin(\alpha \sin(\beta_b)) - \cos(\alpha) \sin(\beta_b) \cos(\alpha \sin(\beta_b)) \quad (2.8)$$

$$z = \cos(\beta_b) \cos(\alpha \sin(\beta_b)) \quad (2.9)$$

where design parameter β_b is the base cone angle and variable α is the angle through which the taught cord unwraps from the base cone.

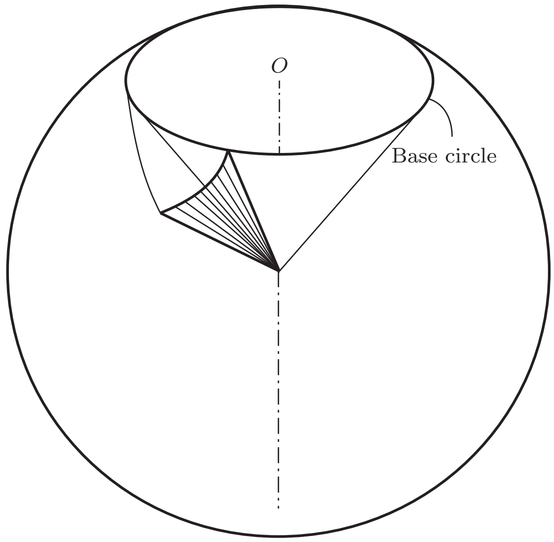

Figure 2–6: Exact spherical involute

An in-house algorithm developed by Angeles et al. was used to produce the ESI tooth profile for the Linamar bevel gear set [37]. The volume of the differential assembly was kept constant for the TA and ESI bevel gear set. The number of pinion and gear teeth, pressure angle, tooth thickness and cone angles where all kept the same. The input data are provided in table 2–4.

Table 2–4: ESI bevel gear set parameters

number of pinion teeth	9
number of gear teeth	14
pressure angle (°)	24°
sphere radius (mm)	46.7805
face width (mm)	22.5

2.4 Tooth Modelling and Bending Stress Calculation

Tooth breakage is a major cause of failure in gears. It occurs as a result of repeated high stresses close to the stress limits, causing bending fatigue. Evaluating tooth bending strength is therefore of high significance. Often tooth breakage happens at the fillet region of the gear. A crack initiates in the fillet region and propagates until breakage occurs. As a result the stress at the fillet region is an indicator of the gear bending strength.

In practice, standards like the ISO and AGMA are widely used for gear-strength evaluation. These methods use simplified formulas that estimate fillet stresses within acceptable limits and in a less expensive procedure. They use different methods and models to generate different design solutions for the same gear under the same operating conditions. Most standards evaluate the gear bending or tooth-root strength by determining the maximum stress in the stretched fillet when a load is applied at the highest point of single tooth contact (HPSTC). However, the location of the critical section in the tooth fillet and the parameters of the critical section are usually different. In this section an overview of the AGMA standards [5] for the evaluation of tooth-root strength in gears is given.

In the AGMA standard, the gear tooth is treated as a cantilever beam with a load applied at the HPSTC. The Lewis method is used to determine the critical section location in the fillet. A constant strength parabola is inscribed within the tooth profile and the tangency points with the fillet are considered the critical section points C. Given a load F applied at an angle α_F, the vertex of the parabola is positioned at the intersection between the applied load line of action and the tooth

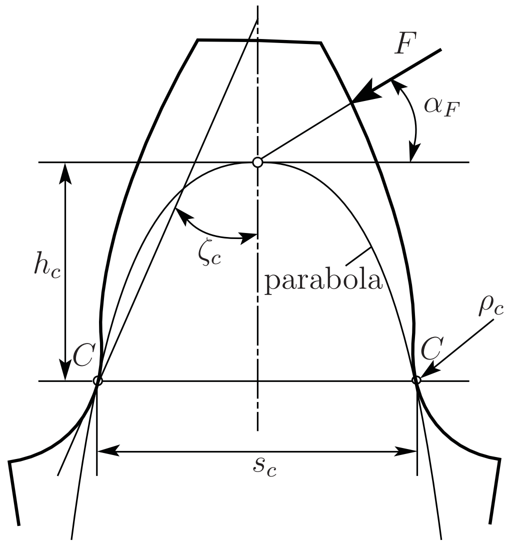

Figure 2–7: AGMA critical section parameters

vertical axis. The parameters of the critical section that are used to calculate the fillet stress are the angle between the tangent to the fillet at the critical point and the centerline ζ_c, tooth thickness at the critical section s_c, bending moment arm h_c, and the radius of curvature of the fillet curve ρ_c at the critical point, as shown in Fig. 2–7. Coefficients accounting for the stress concentration induced by a geometric notch and the geometric properties of the fillet go into the calculation of the local tooth-root stress.

The stress correction factor K_f,

$$K_f = H + \left(\frac{s_c}{\rho_c}\right)^L \left(\frac{s_c}{h_c}\right)^M \tag{2.10}$$

where $H = 0.331 - 0.436\alpha_n$; $L = 0.324 - 0.492\alpha_n$; $M = 0.261 + 0.54\alpha_n$; and α_n is the normal pressure angle.

The bending strength geometry factor J is

$$J = \frac{1}{K_f \dfrac{\cos\alpha_F}{\cos\alpha_n}\left[\dfrac{6h_c}{s_c^2} - \dfrac{\tan\alpha_F}{s_c}\right]} \tag{2.11}$$

The local tooth-root stress σ_c is, in turn,

$$\sigma_c = \frac{F_t P_d}{bJ} \tag{2.12}$$

where F_t is the tangential load; P_d is the diametral pitch; b is the face width.

Load factors are also implemented to account for overload that could be a result of misalignments in the transmission, dynamic loads, etc. They have not been shown in the equation here for simplicity.

Standards like ISO and AGMA estimate fillet stresses. However, to accurately determine the stress distribution in the fillet region, either experimental or numerical methods should be used. Several experimental methods are reported in the literature using electric resistance wire strain gauges or photo-elasticity. Computer-based methods such as the Finite Element Method (FEM) have been widely used in the literature because of their high accuracy. Other methods such as the finite prism method or the theory of Muskhelishvili applied to circular elastic rings have also been reported [5].

The Finite Element Method offers a robust evaluation of the stress distribution in the fillet. Stress in the fillet region depends on a relation between the load applied to the gear tooth and the resulting displacements. In the FEM, the model is discretized into finite elements connected at nodal points and boundaries. Element matrices are obtained by formulating an approximate solution over each element. By combining element matrices, a global stiffness matrix is generated, which governs the force displacement relation over the entire domain [38]. The FEM can be used to accurately determine the tooth-root stresses for complex fillet shapes; hence, it is used in this work.

CHAPTER 3
Methodology

3.1 Curve Synthesis

In the curve synthesis procedure described here, we resort to non-parametric cubic splines to discretize the tooth-root fillet. There are several forms of curve discretization available, including Basis splines and Bézier curves; however, non-parametric cubic splines are chosen because they are the simplest and most straightforward to use, thereby streamlining the procedure. In this chapter two kinds of curves are synthesized, planar and spherical.

3.1.1 Planar-curve Synthesis

Figure 3–1 includes a sketch of the blending segments—the involute and part of the dedendum circle—by means of a third one, Γ. The coordinate frame $\{E\ x_E\ y_E\}$ is built with its origin lying on the projection of $\overline{OD}$ and the x_E-axis coinciding with point B, as shown in Fig. 2–3. Point B, the starting point of the fillet curve, lies on the base circle, while point D, the ending point of the fillet curve, lies on the dedendum circle. Point A is defined as the intersection of the involute with the addendum circle. The tooth-root lies between the base circle and the dedendum circle. Notice that the segments in Fig. 3–1 pertain to a tooth in the lower half of the gear, as opposed to the tooth of Fig. 2–3, for ease of representation.

We define $n+2$ points $\{P_k\}_0^{n+1}$ along Γ, by their polar coordinates $P_k(\rho_k, \theta_k)$, with $P_0(\rho_0, \theta_0) = B$ and $P_{n+1}(\rho_{n+1}, \theta_{n+1}) = D$. For point P_k, let $\theta_k = \theta_0 + k\Delta\theta$, for

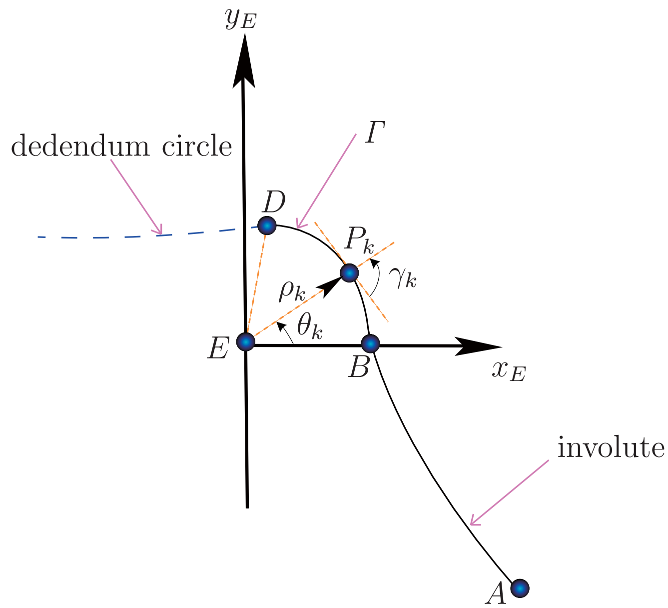

Figure 3–1: The blending of the involute and root circle segment using G^2-continuous curve fillet

$k = 1, 2, \cdots, n+1$, the uniform increment $\Delta\theta$ being

$$\Delta\theta = \frac{\theta_{n+1} - \theta_0}{n+1} \tag{3.1}$$

Hence, the polar coordinates $\{\rho_k\}_1^{n+2}$ are assembled into a $(n+2)$-dimensional vector array as

$$\boldsymbol{\rho} = [\rho_0, \rho_1, \cdots, \rho_{n+1}]^T \tag{3.2}$$

Similarly, its first- and second-order derivatives $\boldsymbol{\rho}'$ and $\boldsymbol{\rho}''$, with respect to the polar coordinate θ of Fig 3–1 are defined likewise,

$$\boldsymbol{\rho}' = \left[\rho_0', \rho_1', \cdots, \rho_{n+1}'\right]^T \tag{3.3}$$

$$\boldsymbol{\rho}'' = \left[\rho_0'', \rho_1'', \cdots, \rho_{n+1}''\right]^T \tag{3.4}$$

According to the definition of non-parametric cubic splines, the cubic polynomial $\rho_k(\theta)$ between two consecutive supporting points P_k and P_{k+1} takes the form [39]

$$\rho_k(\theta) = A_k(\theta - \theta_k)^3 + B_k(\theta - \theta_k)^2 + C_k(\theta - \theta_k) + D_k \tag{3.5}$$

in which $\theta_k \leq \theta \leq \theta_{k+1}$ and $0 \leq k \leq n$.

By virtue of the G^2-continuity condition, i.e., two curvatures coinciding at the blending point, $\boldsymbol{\rho}$, $\boldsymbol{\rho}'$ and $\boldsymbol{\rho}''$ are found to satisfy the linear relationships below [39]:

$$\mathbf{A}\boldsymbol{\rho}'' = 6\mathbf{C}\boldsymbol{\rho}, \quad \mathbf{P}\boldsymbol{\rho}' = \mathbf{Q}\boldsymbol{\rho} \tag{3.6}$$

with matrices $\mathbf{A}$, $\mathbf{C}$, $\mathbf{P}$ and $\mathbf{Q}$ provided in the Appendix.

Further, the curvature at P_k takes the form

$$\kappa_k = \frac{\rho_k^2 + 2(\rho_k')^2 - \rho_k\rho_k''}{[\rho_k^2 + (\rho_k')^2]^{3/2}} \tag{3.7}$$

Now, let the curve Γ be the curve with the "smallest possible curvature", i.e., with a curvature distribution that carries the minimum rms value in the segment comprised between B and D of Fig. 2–3. Hence, the optimization problem is formulated as

$$z = \frac{1}{n}\sum_{k=1}^{n} w_k\kappa_k^2 \longrightarrow \min_{\boldsymbol{\rho}} \tag{3.8}$$

subject to

$$\kappa_0(\rho, \rho', \rho'') = \kappa_B = 0, \quad \kappa_{n+1}(\rho, \rho', \rho'') = \kappa_D = \frac{1}{r_d} \tag{3.9}$$

in which $w_k > 0$ denotes the normalized weight at point P_k, obeying $\sum_{k=1}^{n} w_k = 1$.

Besides, with reference to Fig. 2–3, the additional boundary constraints at the two blending points are

$$\begin{cases} \theta_0 = \theta_B = 0 \\ \theta_{n+1} = \theta_D = \dfrac{\pi}{2} - \zeta_m \end{cases}, \quad \begin{cases} \rho_0 = \rho_B = r_b \tan \zeta_m \\ \rho_{n+1} = \rho_D = \dfrac{r_b}{\cos \zeta_m} - r_d \end{cases} \tag{3.10}$$

The optimization problem thus formulated is constrained and nonlinear, which can be solved using a suite of methods; the one used here is the ODA (orthogonal decomposition algorithm) [40], as implemented in MATLAB.

3.1.2 Spherical-curve Synthesis

The foregoing curve synthesis procedure is used for spur and bevel gears tooth-root profile optimization. While its implementation is obvious in the spur gear case, in bevel gears it depends on the method of generation. In this research work the TA and the ESI tooth profile have been considered for bevel-gear generation.

The projection of a TA bevel gear onto the Tredgold plane, tangent to the back cone, generates a *virtual* spur gear, as shown in section 2.2. The curve-synthesis procedure is implemented on the tooth-root profile of the virtual spur gear. Upon regeneration of the bevel gear using the corresponding virtual spur gear with optimum tooth-root fillet profiles, the bevel gear tooth-root profile is smoothed.

On the other hand, if the tooth flanks are designed with an ESI profile, then the tooth-root profile also lies on a spherical surface. Here we resort to the parametrization of a spherical curve.

Figure 3–2 includes the sketch of a bevel gear tooth with an ESI and the dedendum circle, which is the intersection of the dedendum cone with the sphere surface.

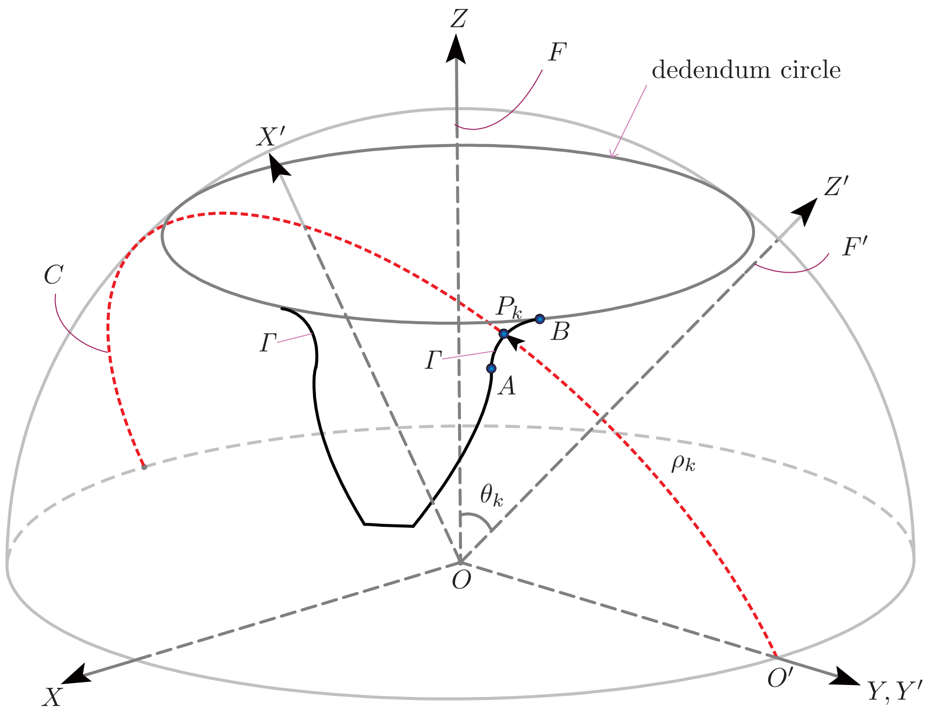

Figure 3–2: The blending of the involute and the root circle segment of an exact spherical involute bevel gear

The spherical curve Γ blends the ESI and the dedendum circle. The point O' is defined at the intersection of the sphere and the Y-axis. Point A, the starting point of the fillet curve, lies on the base circle, while point B, the ending point of the fillet curve, lies on the dedendum circle.

To define the position of any point P_k on the fillet curve, we introduce the angle θ_k between the Z-axis and the normal to the plane of the great circle C (Z') that passes through points O' and P_k, and the arc length ρ_k on the great circle, namely, the length of the shortest path or the *smaller geodesic* between the two points. The shortest path in spherical geometry is the equivalent of a straight line in Euclidean geometry.

Now, $n+2$ points are defined along Γ with $P_0 = A$ and $P_{n+1} = B$. The problem is treated like a planar one but by using the arc length ρ and the angle θ to define the position of the supporting points. The optimization problem is formulated as

$$z = \frac{1}{n}\sum_{k=1}^{n} w_k \kappa_k^2 \longrightarrow \min_{\boldsymbol{\rho}} \tag{3.11}$$

subject to

$$\kappa_0(\rho, \rho', \rho'') = \kappa_A = 0, \quad \kappa_{n+1}(\rho, \rho', \rho'') = \kappa_B = \frac{1}{r_d} \tag{3.12}$$

in which r_d is the radius of the dedendum circle and $w_k > 0$ denotes the normalized weight at point P_k, obeying $\sum_{k=1}^{n} w_k = 1$.

With reference to Fig. 3–2, the additional boundary constraints at the two blending points are

$$\begin{cases} \theta_0 = \theta_A \\ \theta_{n+1} = \theta_B \end{cases}, \quad \begin{cases} \rho_0 = \rho_A \\ \rho_{n+1} = \rho_B \end{cases} \tag{3.13}$$

The optimization problem is solved. To generate the fillet curve, the resulting supporting points which are defined in terms of arc length ρ and angle θ are defined using Cartesian coordinates and input to a CAD software to generate the spherical curve. Using a simple rotation the transformation can be done. With reference to Fig. 3–2, the frame F' is attached to the great circle C, its Y'-axis always coincident with the Y-axis. A matrix $\mathbf{R}$ represents the rotation of frame F' with respect to frame F about the Y-axis, namely,

$$\mathbf{R} = \begin{bmatrix} \cos\theta & 0 & -\sin\theta \\ 0 & 1 & 0 \\ \sin\theta & 0 & \cos\theta \end{bmatrix} \tag{3.14}$$

The position vector of the point P_k that lies on the great circle C, in frame F', is given by

$$\mathbf{r}'_P = \begin{bmatrix} r\sin\dfrac{\rho}{r} & r\cos\dfrac{\rho}{r} & 0 \end{bmatrix}^T \tag{3.15}$$

where r is the sphere radius. The subscript k has been suppressed for simplicity. Therefore, the position vector of point P_k can be expressed in frame F by

$$\mathbf{r}_P = \mathbf{R}\mathbf{r}'_P \tag{3.16}$$

thus obtaining

$$\mathbf{r}_P = \begin{bmatrix} r\cos\theta\sin\dfrac{\rho}{r} \\ r\cos\dfrac{\rho}{r} \\ r\sin\theta\sin\dfrac{\rho}{r} \end{bmatrix} \tag{3.17}$$

3.2 Co-simulation

The structural optimization problem is implemented via co-simulation among: the ODA package, implemented in Matlab; modelling, using SolidWorks Application Programming Interface (API); and FEA, using a customized ANSYS Parametric Design Language(APDL). The iterative design optimization procedure for gear tooth-root profile optimization is shown in the flowchart of Fig. 3–3. In the spur gear case, both modelling and FEA were done on ANSYS using APDL. However, bevel-gear modelling, which requires more advanced solid modelling techniques, was implemented using a customized macro in VisualBasic.NET format on SolidWorks. The software packages were coupled together to interact in an automated iterative procedure to solve the structural optimization problem.

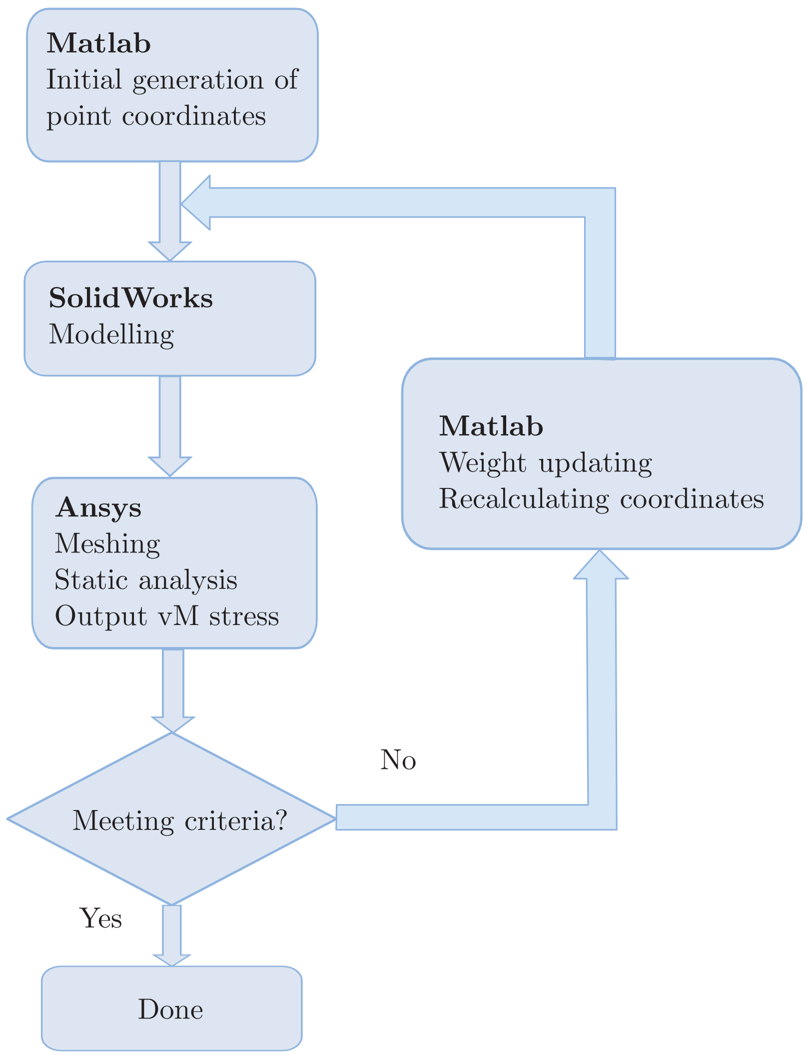

Figure 3–3: Root curve optimization flowchart

The procedure starts with all the weight coefficients, w_k, equal to $1/n$ and the foregoing optimization problem is solved. The supporting-point coordinates are obtained and used to generate the initial cubic-spline tooth-root profile, called the *geometrically* optimum fillet. It is so termed because it was obtained with equal weights. As a result of the G^2-continuity offered by the geometrically optimum fillet, the stress distribution in the tooth-fillet region is reduced significantly. However, further reduction is still possible through an iterative procedure.

The supporting-point coordinates of the geometrically optimum fillet obtained from Matlab are imported into ANSYS (in the spur gear case) or SolidWorks (in the bevel gear case), where the gear tooth is modelled. A FEA is then carried out on the gear model on ANSYS. The gear tooth is meshed, displacement constraints and loading conditions are applied, and the FEA is conducted. Based on the von Mises stress distribution in the fillet thus obtained, the weight coefficients are determined and used for the next iteration, such that:

$$w_k = \frac{s_k}{\sum\limits_{i=1}^{n} s_i} \tag{3.18}$$

where s_k is the von Mises stress at the k^{th} supporting point.

The definition for weight coefficients given above ensures that the higher the stress at a supporting point, the more it is penalized. The problem previously formulated is solved again but with non-uniform weight coefficients until the maximum von Mises stress remains almost constant. The process helps approach the Venkayya criterion of acheiving an almost unifrom stress distribution at the critical region of the fillet [14]. The final fillet shape is called the *structurally* optimum fillet.

An important aspect of structural optimization problems pertains to the loading conditions [11]. A gear tooth is subject to variable loading conditions because the contact point between a pair of gear teeth changes during the process of gear meshing. The geometrically optimum fillet offers a significant reduction of the stress distribution in the fillet and does not depend on the loading conditions. On the contrary, the structurally optimum fillet depends on the loading conditions, i.e., a structurally optimum tooth-root profile under one loading condition is not necessarily optimum for another loading condition. However, the maximum tooth-root stress occurs when the tooth is loaded at the HPSTC [41]. Thus, in this work the structurally optimum tooth-root profile was computed at that loading position.

Furthermore, the load was selected arbitrarily. As the material is assumed to operate in the linearly elastic region, any load below yield conditions should produce the same desired result, namely, a comparison between the smoothed and circular fillet.

3.3 CAD Modeling

Precise CAD modelling is necessary in shape optimization problems to accurately represent the geometry. The model generated is used for carrying out finite element analysis to investigate the effect of geometry modifications on the stress distribution, imprecise modelling thus giving rise to misleading results. In this research accurate representation of the tooth, especially the fillet profile, is necessary. Different geometric and solid modelling techniques are used for spur and bevel gears.

The plane stress model is the most suitable for the strength analysis of spur gears. The conditions for 2D strength analysis are met. The gear face width is much smaller than the pitch diameter (in-plane dimension), same shape in each transversal section and a uniform load distribution along the tooth line [5]. Hence a 2D geometric model was generated. The spur gear model was generated in ANSYS 14.0. Considering the geometric symmetry of the gear, a single tooth was modeled and used for FEM computations. A precise representation of the whole tooth profile was based on non-parametric cubic splines by means of the *spline* function rather than on B-splines (by means of the *bsplin* function) because the former is more suitable for the problem at hand. While a cubic spline is composed of piecewise third-order polynomials that pass through the supporting points, a B-spline best fits a curve to the supporting points. More importantly, the meshing process is facilitated when using cubic splines because the boundary nodes are automatically selected to coincide with the supporting points. Details on the meshing process are explained in Section 3.4. Considering the symmetry of the gear tooth, one side of the tooth was generated and then reflected about the axis of symmetry. The spur gear tooth model is shown in Fig. 3–4.

A 3D FEA of the same spur gear under the same operating conditions was also conducted by Zou et al. [4]. The same results were obtained for the 2D and 3D models, which confirmed the accuracy of the FEA.

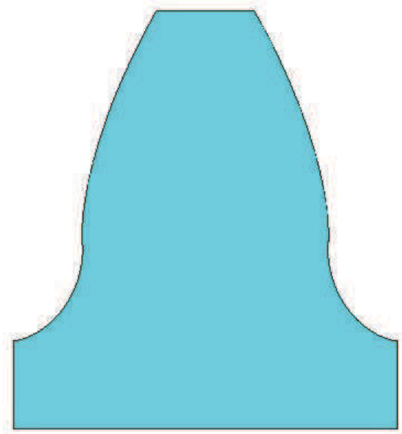

Figure 3–4: Spur gear tooth model

Considering the limitations in solid modelling features available in classical ANSYS, we resort to SolidWorks for generation of 3D bevel-gear models, geometrically more complex than spur gears. Upon examination, it was found that the existing bevel gear models available in the SolidWorks 2013 toolbox inaccurately represent the geometry. Mainly, the tooth profile is represented as a circular arc instead of a circle involute.

A combination of modelling features was used to generate the bevel gear. The TA and the ESI bevel gears were both modelled. To model the former, first the cross section of the gear is constructed using the basic dimensions evaluated in section 2.2. The cross section is rotated about the gear axis to generate the main body, which is conical. The virtual spur gear on the Tredgold plane is then used to create the tooth cut. The Tredgold plane is defined by imposing a tangency constraint with the back cone. A 2D sketch of the tooth space of the virtual spur gear is created on the Tredgold plane using the spline function offered by SolidWorks (which is a B-spline),

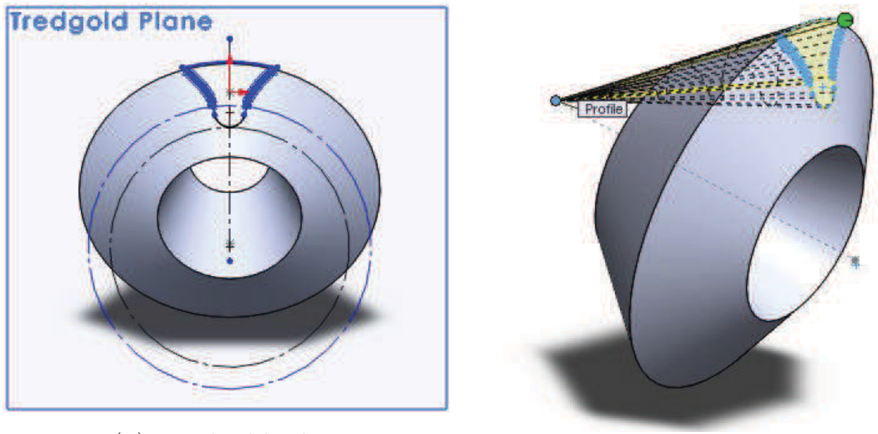

(a) Tredgold Plane
(b) lofted cut

Figure 3–5: TA bevel gear CAD modelling

to generate the involute and tooth-root profile. The tooth cut shape is tapered smoothly towards the apex and used to cut the gear using the *lofted cut* feature as shown in Fig. 3–5. Through rotation copying the tooth spaces, the full gear geometry was accomplished. Both the pinion and the gear belonging to the differential gear set manufactured by Linamar were generated. The assembly is shown in Fig. 3–6.

The Linamar differential gear set was also modelled with bevel gears having an ESI tooth profile. The volume enclosed by the TA bevel gear set was used to calculate the radius of the sphere enclosing the ESI gear set. The gear cross-sectional area is constructed such that, upon rotation about the main axis, a spherical boundary is generated (rather than a conical one). The ESI tooth profile is generated using the algorithms proposed by Angeles et al. [37] and implemented in Matlab. The spherical involute and fillet profile data points are then imported into SolidWorks to construct the tooth cut profile which lies on the sphere. Using the lofted cut feature,

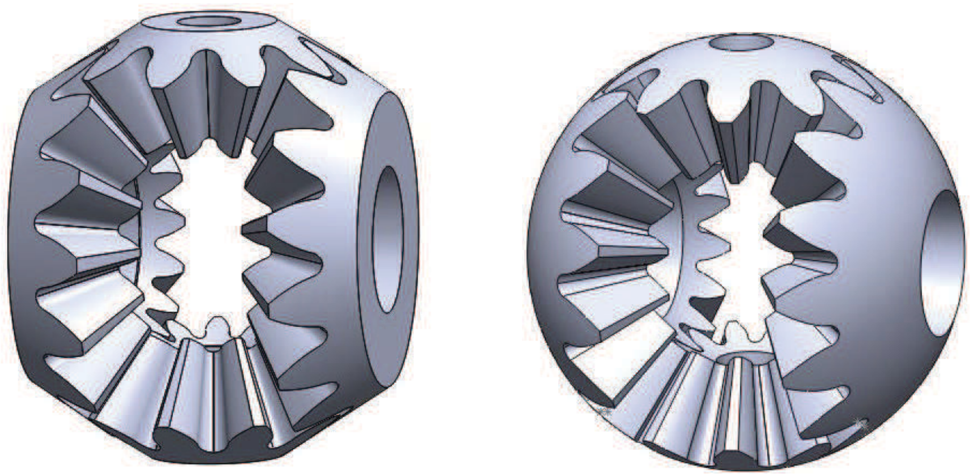

(a) Tredgold approximation

(b) exact spherical involute

Figure 3–6: Linamar differential gear set

the tooth spaces in the bevel gear are generated and finally repeated in a circular pattern to render the full gear geometry.

3.4 Finite Element Models

The material used in the FE analyses conducted in this research is structural steel with a Young modulus of 2.1×10^{11} Pa, a Poisson ratio of 0.3, and a density of 7870 kg/m^3. The gear models were based on the assumption that the material is homogeneous and isotropic i.e., free of damages or imperfections, scratch and machining marks, etc.

As shown in Fig. 3–7, quadratic 4-node PLANE182 elements were used on ANSYS 14.0 to discretize the spur-gear tooth domain. An important issue that should be addressed in structural analysis is the remeshing problem. During the optimization procedure, the fillet profile is modified; it is therefore necessary to accurately remesh the model for further evaluation. The choice of cubic splines to represent the tooth profile was essential to achieving an efficient and accurate mesh, because the spline passes through the supporting points. Upon meshing, the boundary nodes are automatically selected by the FE software to coincide with the supporting points, the mesh thus being adaptive to profile modifications. Additionally, a finer mesh is generated at the tooth-root where 50 supporting points were used to represent the profile and where the stress values at the nodes are of particular interest to the topic. A rougher mesh was generated at the involute tooth section and the gear rim. An average of 3363 elements and 3490 nodes were used in creating the mesh for the tooth models with different fillet shapes.

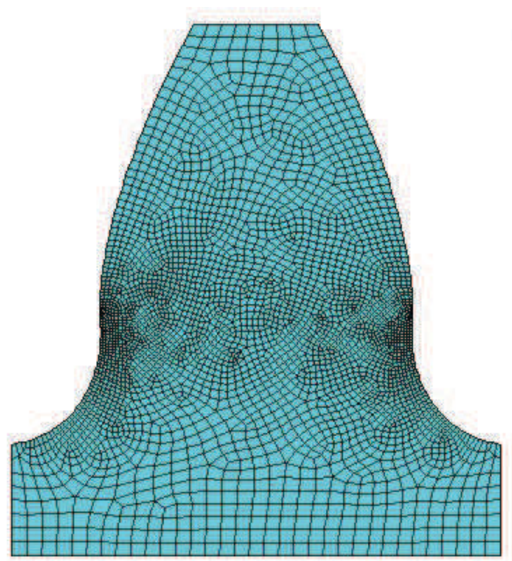

Figure 3–7: Spur gear tooth mesh

The boundary conditions on the generated FE model are defined by displacement constraints over the inner tooth hub and cut boundaries, which separate the modeled gear tooth from the rest of the gear body. A $1000(\cos 20°)$ N tangential load that the gear transmits is applied as an external force on the FE model, at its HPSTC, uniformly distributed along the contact line over the tooth width.

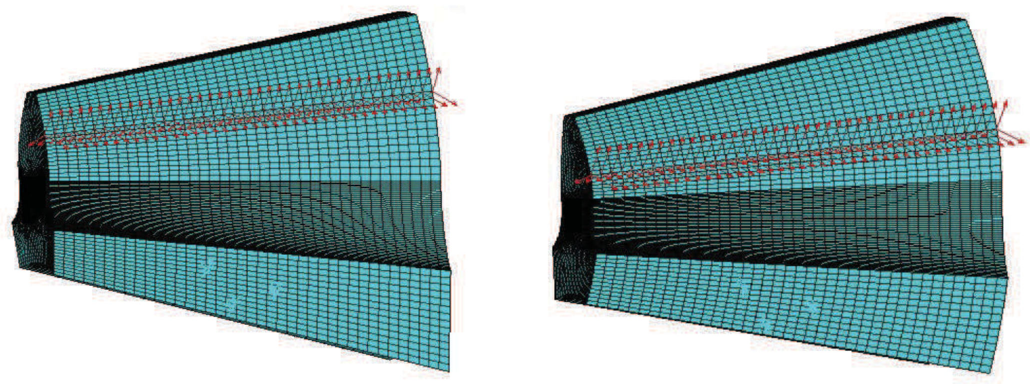

(a) TA gear tooth

(b) ESI gear tooth

Figure 3–8: Bevel gear tooth mesh

The bevel gear tooth models generated on SolidWorks are imported into ANSYS as IGES files, to be used for FEA. IGES is a very rich file format; however, not all entity types are supported by every CAD system. The imported tooth models are therefore modified to construct missing surfaces or to repair incomplete entities.

The tooth is meshed using 8-node brick SOLID185 elements which are suitable for the 3D modelling of solid structures. The sweep-mesh approach is used to sweep the mesh from the tooth heel through the volume (to the toe). The remeshing problem is also addressed here. The tooth profile curves in the wire-frame imported from SolidWorks are free of the supporting points. Therefore, upon meshing, the boundary nodes do not necessarily coincide with the original supporting points, which is necessary for the structural analysis procedure. Hence, an angular element size is imposed on the fillet curve mesh, i.e., the number of angular divisions on the fillet curve is kept constant such that each of the fillet nodes coincide with the corresponding supporting point. This is imposed on the tooth fillets on both the heel and toe side such that upon sweep there will be the same number of nodes on each side. Even though the generating tooth cut profile is on the heel side, the maximum stress is often in the toe; therefore, the number of nodes in the fillets in each transversal section should be kept constant. A rougher mesh is used for the involute tooth and the rim to save computation time. The average number of elements used was 137,553. The displacements over the inner tooth hub and the cut boundaries of the bevel gear tooth were constrained. A $1000(\cos 20^{\circ})$ N tangential load is applied as an external force on the FE model, at its highest line of single tooth contact (HLSTC). The FE models for ESI and TA bevel gear teeth are shown in Fig. 3–8.

CHAPTER 4
Results

In each iteration of the optimization procedure, FEA was conducted to evaluate the von Mises stress distribution in the gear tooth-root. The FEA results obtained for spur and bevel gears are reported in this chapter. The stress distribution in the optimum fillets are also compared with their circular-filleted counterpart.

4.1 Spur Gears

The maximum von Mises stress in the spur gear tooth-root versus the number of iterations is shown in Fig. 4–1. The optimization procedure stopped in the seventh iteration, when the maximum von Mises stress reduced from the previous iteration is smaller than 0.01 MPa. Starting from an initial guess, the maximum von Mises stress drops significantly in the first and second iterations and then settles to a value about 1.5% above the minimum achieved in iteration 2.

The fillet obtained in the first iteration is the geometric optimum, obtained with equal weighting factors. The structurally optimum fillet is implemented after six more iterations (iteration 7), although the second iteration produced already a lower maximum von Mises stress, because a more uniform stress distribution is achieved with the former. A plot of the optimum fillet profiles is shown in Fig. 4–2. The von Mises stress distributions of the optimum fillets are shown in Fig. 4–3.

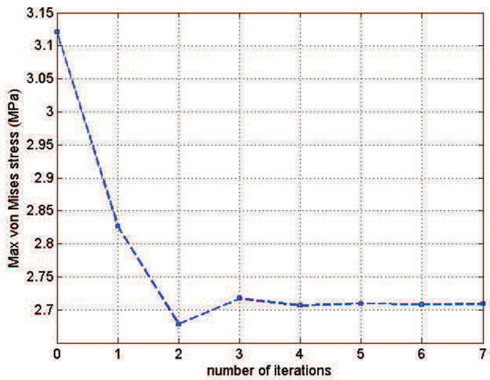

Figure 4–1: maximum vM Stress vs. number of iterations

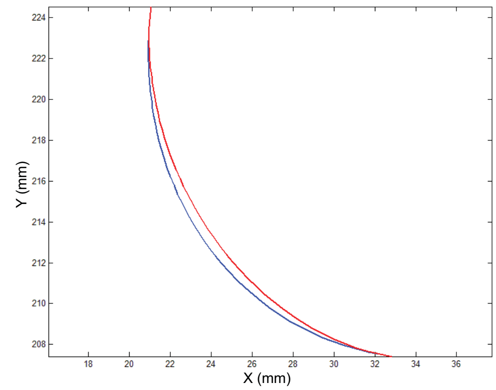

Figure 4–2: Fillet profiles; geometrically optimum (blue) and structurally optimum (red)

The von Mises stress distribution in the circular-filleted tooth-root has also been evaluated, as shown in Fig. 4–4. Compared to its circular-filleted counterpart, the geometrically optimum fillet offers a 16.5% reduction rate in the maximum von Mises stress, while the structurally optimum offers a 20.0% reduction. The maximum von Mises stress values are given in Table 4–1.

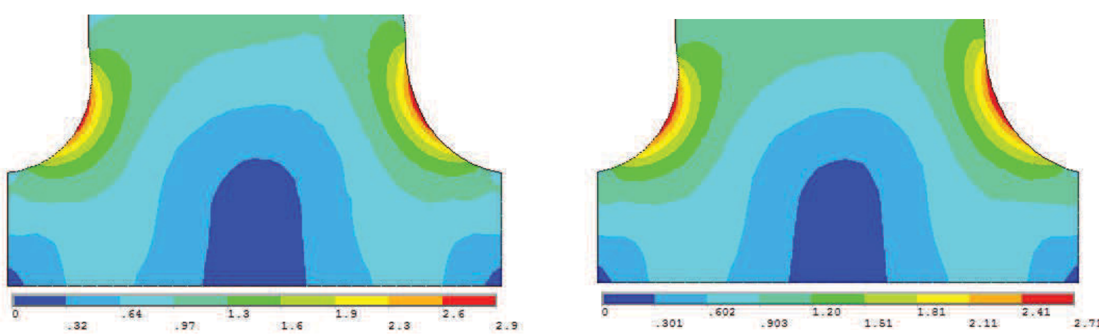

(a)

(b)

Figure 4–3: vM stress distribution plots for (a) geometrically optimum (b) structurally optimum fillet

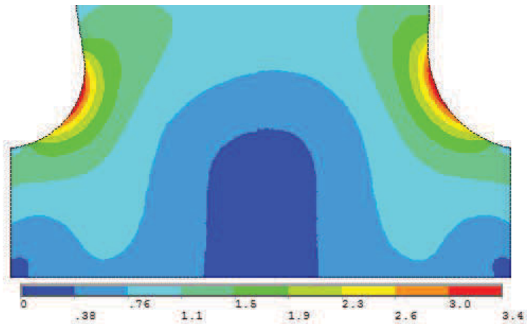

Figure 4–4: vM stress distribution for circular fillet

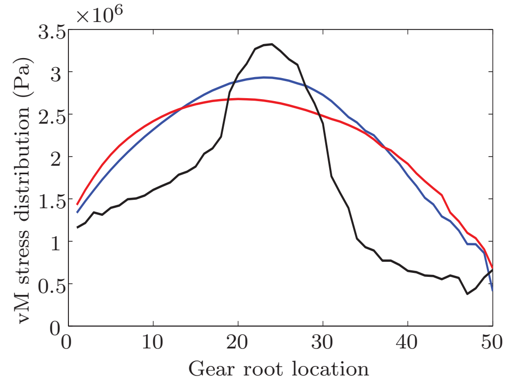

Figure 4–5: vM stress distribution on circular (black), geometrically optimum (blue) and structurally optimum (red) fillets

Additionally, the von Mises stress distribution of the three fillet curves is plotted in Fig. 4–5, in which the abscissae denotes the node number along the gear tooth-root profile. The results show that a more uniform stress distribution is achieved in the optimum fillets, thereby meeting the design objectives.

Table 4–1: Maximum von Mises stress in different tooth-root curve types

root curve type	von Mises σ_{vm} (MPa)
Circular	3.386
Cubic spline (geometrically optimum)	2.827
Cubic spline (structurally optimum)	2.709

4.2 Bevel Gears

The FEA results for TA and ESI bevel gears are reported in this section.

4.2.1 Tredgold Approximation

Figure 4–6 shows a plot of the maximum von Mises stress in the TA bevel gear tooth-root versus the number of iterations. The optimization procedure stopped in the sixth iteration. A similar behaviour is observed here: starting from an initial guess, the maximum von Mises stress drops significantly in the first and second iterations and then settles to a value about 0.6% above the minimum achieved in iteration 2.

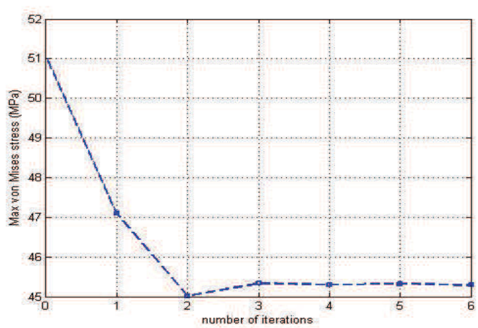

Figure 4–6: maximum vM Stress vs. number of iterations

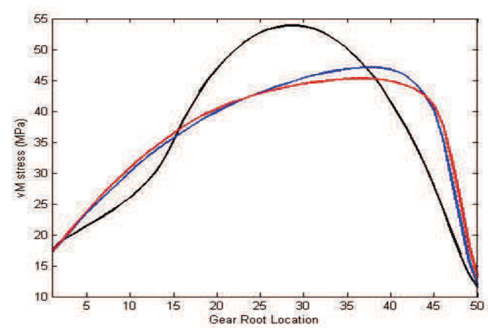

Figure 4–7: vM stress distribution on circular (black), geometrically optimum (blue) and structurally optimum (red) fillets

The von Mises stress distributions of the circular, the geometrically optimum (iteration 1) and the structurally optimum (iteration 6) fillets are shown in Fig. 4–8, and the maximum von Mises stress values are given in Table 4–2. The von Mises reduction rate is 12.6% in the geometrically optimum fillet and 15.9% in its structurally optimum counterpart, compared with the circular-filleted tooth-root.

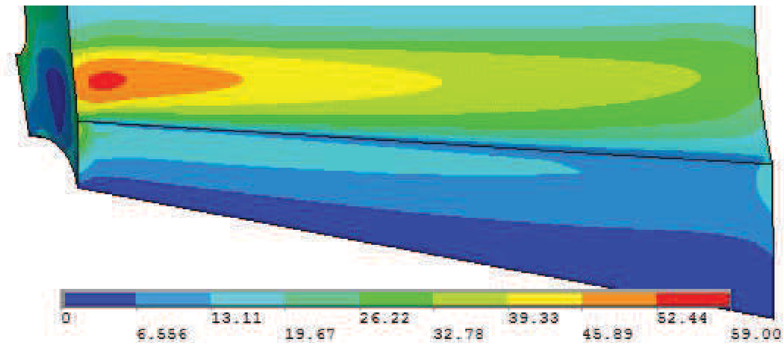

(a) Circular fillet

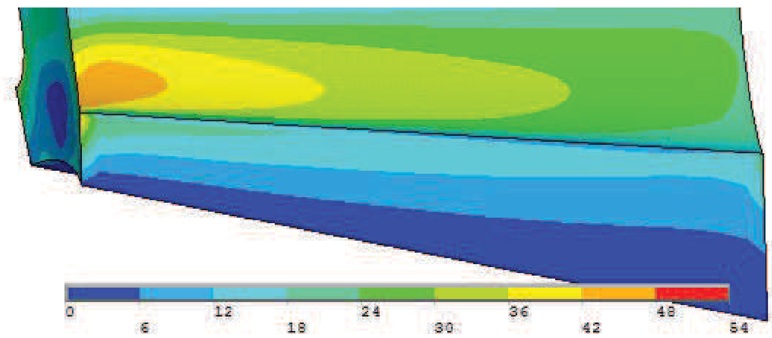

(b) Geometrically optimum fillet

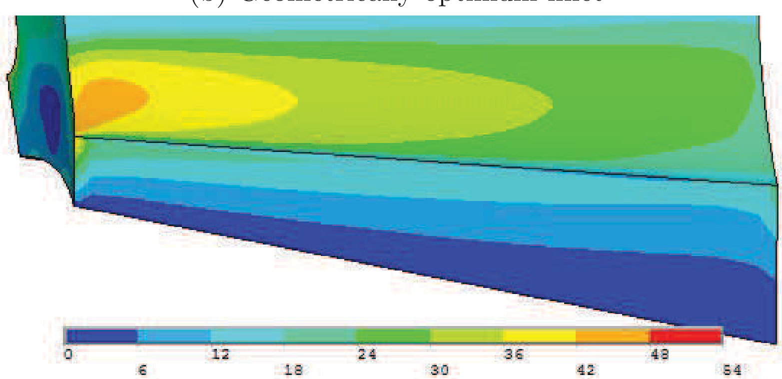

(c) Structurally optimum fillet

Figure 4–8: von Mises stress distributions for various fillets

Table 4–2: Maximum von Mises stress in different tooth-root curve types

root curve type	von Mises σ_{vm} (MPa)
Circular	53.88
Cubic spline (geometrically optimum)	47.093
Cubic spline (structurally optimum)	45.294

To show the von Mises stress distribution along the fillet boundary, that of the three fillet curves are plotted in Fig. 4–7, in which the abscissa denotes the node number along the gear tooth-root profile.

4.2.2 Exact Spherical Involute

The optimization procedure for the ESI bevel gear fillet stopped at the eighth iteration as shown in Fig. 4–9. From the initial guess, a significant decrement is observed in the maximum von Mises stress in the first and second iterations and then settles to a value about 1.5% above the minimum achieved in iteration 2.

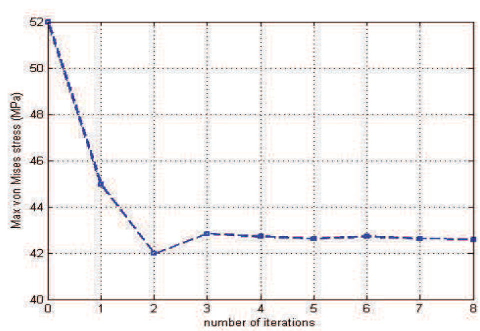

Figure 4–9: maximum vM Stress vs. number of iterations

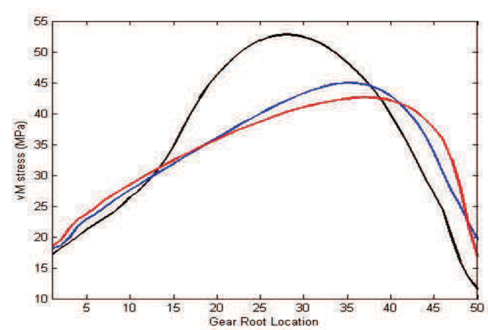

Figure 4–10: vM stress distribution on circular (black), geometrically optimum (blue) and structurally optimum (red) fillets

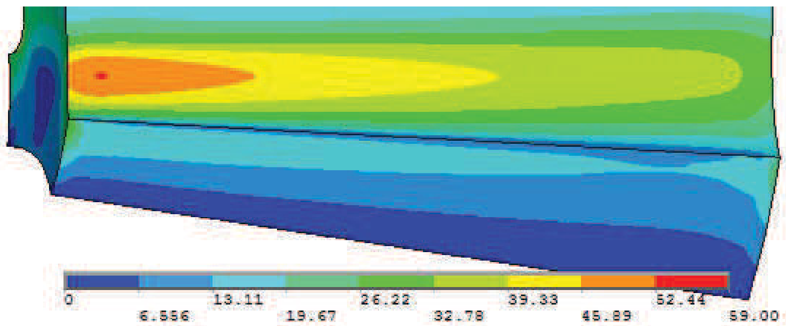

(a) Circular fillet

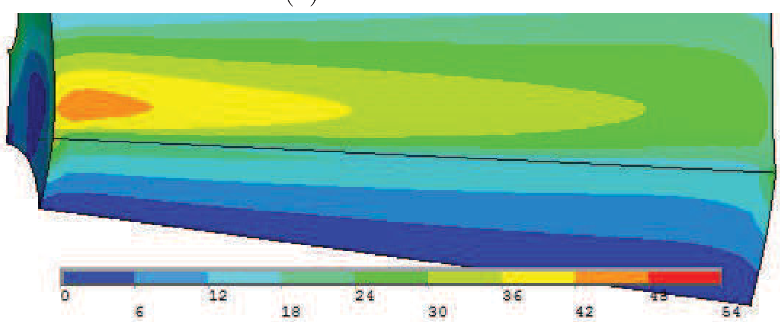

(b) Geometrically optimum fillet

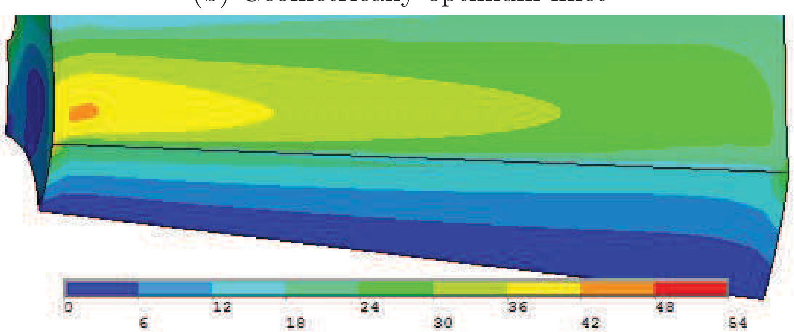

(c) Structurally optimum fillet

Figure 4–11: von Mises stress distributions for various fillets

Table 4–3: Maximum von Mises stress in different tooth-root curve types

root curve type	von Mises σ_{vm} (MPa)
Circular	52.774
Cubic spline (geometrically optimum)	44.948
Cubic spline (structurally optimum)	42.587

The maximum von Mises stress values in the optimum and circular fillets are given in Table 4–3. The von Mises stress reduction rate is 14.83% in the geometrically optimum fillet and 19.30% in the structurally optimum, compared to the circular fillet. The von Mises stress distributions for the three fillets are shown in Fig. 4–11.

Additionally, a more uniform stress distribution is achieved in the optimum fillets when compared to the circular fillet, as shown in Fig. 4–10.

CHAPTER 5
Conclusions and Future Work

Spur and bevel gear tooth-root profile optimization, for maximum load-carrying capacity, was reported in this thesis. Non-parametric cubic splines were used to synthesize G^2-continuous fillets that minimize stress concentrations in the tooth-root region. First a geometrically optimum, then a structurally optimum fillet is synthesized. Compared to its circular-filleted counterpart, the proposed structurally optimum fillet designs offer a 20.0% reduction in the maximum von Mises stress in the tooth-root of spur gears, and 15.9% and 19.3% reduction in TA and ESI bevel gears, respectively. Hence, the von Mises-stress-reduction rates of the proposed designs are significant. It is noteworthy that ESI tooth shapes were originally proposed on kinematics, not strength, considerations, yet bevel gears with ESI teeth outperformed their TA counterparts also in terms of load-carrying capacity. Additionally, the stress distribution of the fillets changed dramatically upon fillet-smoothing. The stress distributions in the proposed fillet shapes were more uniform in comparison with circular fillets.

Static analysis was done in this research to compute stresses in the tooth-root. The proposed tooth-root profile designs offer significant stress reduction in that region. In a dynamic analysis, it is understood that the tooth-root shape affects the dynamic characteristics of a gear system. Although tooth-root stresses are expected to be reduced in dynamic conditions with the proposed designs, a deeper investigation is recommended to calculate the amount of stress reduction achievable with the proposed designs for a specific gear system at different operating speeds.

The manufacturing processes required to produce gears with optimum fillets are outlined in the Appendix. Conventional machining methods may be used to produce the proposed designs; however, changes in the tool geometry and/or generative motion will be necessary. New technologies generically known as additive manufacturing, can also be adopted to manufacture optimum gears. A more in-depth investigation on the feasibility, cost and possibility of mass-production is required to identify the optimum manufacturing methods for spur and bevel gears with the new proposed tooth-root designs.

Appendix A: Manufacturing

Producing gears requires precise manufacturing operations. Conventional machining methods such as broaching or hobbing are widely used because of their high production rates. Gear forming methods such as powder metal technology, sintering, or more generally, additive manufacturing, are also available and gaining broad acceptance. Gear forming methods generally offer freedom in design and can easily accommodate non-standard fillet shapes. Alterations in conventional machining processes may also allow the production of gears with optimum fillets. However, cost considerations and possibility of mass-production scale have to also be taken into account.

Gear Machining Methods

Gear machining methods are classified into gear form-cutting and gear generation.

Gear Form-cutting

In gear form-cutting techniques, form tooth cutters are used that have profiles identical to the space between the gear teeth. By using cutters having tooth space profiles including optimum fillets, gears with such fillets can be formed. Gear form-cutting methods include broaching and milling.

A broach is a multi-tooth cutting tool. Its profile is identical to the space between all gear teeth. Each tooth on the broach is generally higher than the proceeding tooth. In broaching, the broach or the gear blank is pushed or pulled relative to each

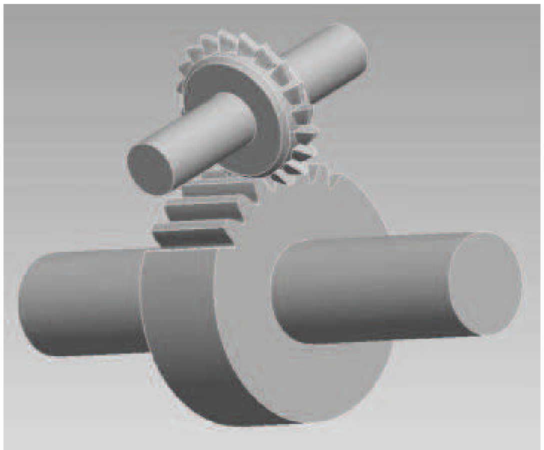

(a) Gear milling

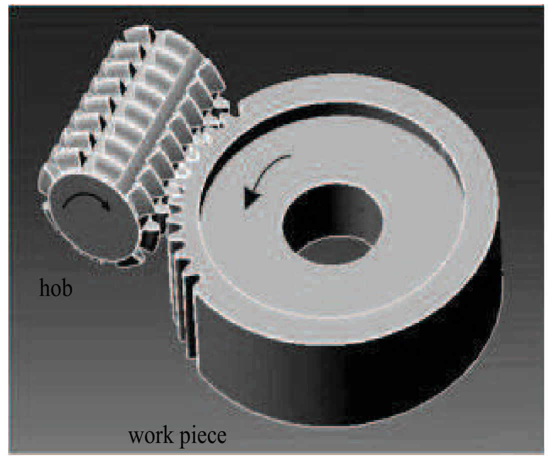

(b) Gear hobbing

Figure 1: Various gear machining methods [1]

other to remove material. The depth of cut, therefore, increases with each tooth as the process is done and the gear is formed all at once.

A multi-edge cutter is used in the milling process to create the tooth space between neighbouring teeth. The cutting tool has a profile identical to the space between two neighbouring teeth. The rotating cutter is gradually fed into the stagnant workpiece to produce each tooth space individually. The process could also be used to machine bevel gears usually on heavy-duty milling machines.

Gear Generation

Gear generation involves gear cutting through the relative motion between a rotating cutting tool and the generating motion or rotation of the workpiece. The root curve depends on the motion program of the cutting tool, gear rotation and tool-tip geometry. The tool profiles used are not identical to the tooth spaces. Using the “gear forms tool” generating method, the gear teeth with optimum fillet profile can be meshed with the cutting tool to generate the corresponding tool profile [27]. The main gear generation methods used are hobbing, shaping and rack generation.

Hobbing is a machining method commonly used for the production of spur and helical gears. The hob is a helical cutting tool. Both the hob and the gear blank rotate as the hob is fed axially into the gear blank.

A pinion-shaped cutter is used in shaping. It is aligned with the gear axis and begins cutting by reciprocating while feeding gradually into the gear blank to a predetermined depth. Both the cutter and the blank rotate at the same pitch circle velocity.

During rack generation, a multi-tooth rack shaped cutter is reciprocated along the axis of the gear blank and fed into it while the blank slowly rotates. Once the cutter finishes a path it is disengaged and returns to a starting point.

Gear Forming Methods

The use of gear forming methods such as powder metal processing, injection molding, forging and others, allow for the production of gears with non-standard optimum fillets. Some of those methods are outlined in this section.

Powder metallurgy (PM) processing uses atomic diffusion to create objects from metal powder at high temperatures. Mass production of gears with optimum fillets is possible using PM. The process is more efficient in producing non-standard gears than traditional cutting methods [32]. Casting methods could be used to produce non-standard gears. Several casting methods are available, including sand, die and investment casting. The accuracy of the gear is dependent on the quality of the die or the mold. Gears made of non-ferrous material such as aluminium and copper alloys are commonly extruded. The teeth are formed on long rods and then cut into usable lengths.

Gearing Industry

Linamar Corporation is a leading designer and manufacturer of precision metallic components, including gears for the automotive and energy industry. Several Linamar facilities in Guelph, ON were visited by the author on July 11th, 2013, together with other members of the APC project team. These facilities included Linamar Gear, one of the largest gear production facilities in North America, and McLaren Performance Technologies, a Linamar subsidiary. A tour of the facilities was done and discussions were conducted with engineers at Linamar, who provided useful insight on the design and manufacturing capabilities of gears in industry.

Linamar designs and manufactures straight, helical and bevel gears for the automotive industry. Gear design is made according to the American Gear Manufacturers Association (AGMA) standards. Most gears are produced according to AGMA 12, 12 denoting the Gear Quality Number; that is a high-accuracy level, achieved by grinding and shaving, with first-rate machine tools and skilled operators. In the design phase, FEA is conducted using ANSOL, a software package. The gear material is chosen and the model is loaded with the operating loading conditions. The software package computes gear stresses at different meshing positions of the gear teeth. If stresses are not within allowable limits, the gear parameters are changed.

In the manufacturing phase, highly automated production lines take the gear blanks through the different stages of the manufacturing process, from cutting, followed by heat treatment, to grinding and shaving and, finally, to measurement, to ensure that the gears fall within the precision standards.

Different methods are used to cut the gear teeth, including hobbing, shaping and broaching. After cutting of the gear teeth, the gears are heat-treated to achieve the necessary hardness, strength and wear resistance for the intended use. To compensate for heat-treatment distortion of a cut gear, grinding is used to ensure that the gear falls within the precision standards. Attention is also given to achieving a smooth surface between the involute profile of the tooth and the fillet.

Finally, gear shaving is used to improve the surface finish of the gear teeth. A few gears are selected randomly from the batch and inspected for accuracy. Special machinery is used that is capable of measuring the geometric accuracy of gears, namely, gear tooth spacing, profile, helix, concentricity, and finish.

A variety of tests on gears are also conducted. In McLaren Performance Technologies, many testing apparatuses are used to test the gears. Most of the time failure in gears occurs as a result of fatigue; therefore, a couple of fatigue tests in addition to a static test are conducted.

Cyclic loading is applied to a gear tooth using the apparatus shown in Fig. 2a to simulate tooth-loading, as it goes in and out of mesh repeatedly with another gear. The tool at the end of the arm in contact with the gear tooth has an involute profile to emulate the same contact loading that occurs in gears. The test is stopped if failure occurs, which is when 10 percent of initial displacement of the arm is detected or if the number of cycles reached a given threshold.

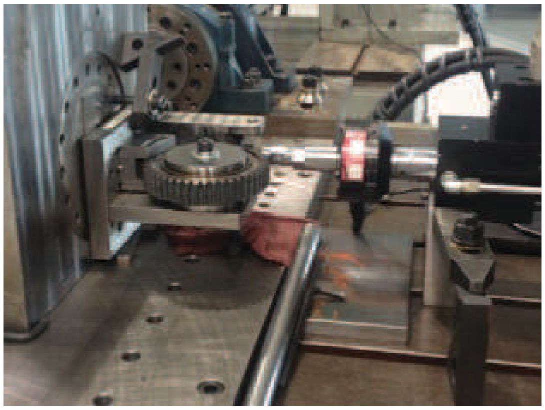

(a) Failure Test

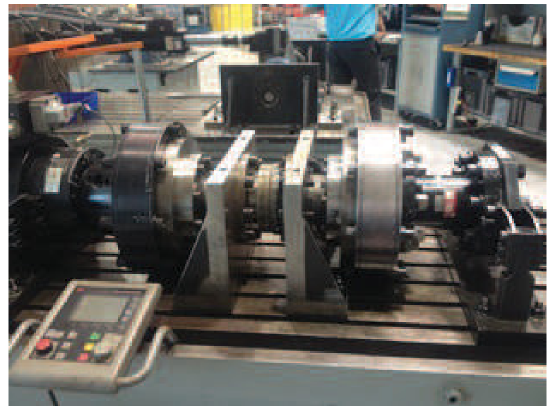

(b) Torque Test

Figure 2: Various tests done on gears

A torque test is also done, in which a cyclic torque is applied to the gear teeth, instead of a force. The test is conducted until either failure occurs or a specified number of cycles is achieved. The apparatus used for this test is shown in Fig. 2b.

A static test is done to determine the maximum static load that a gear tooth can withstand before failure. A high capacity press is used for this test. High loads are applied to the gear tooth until failure happens.

Appendix B: Matrices Related to the G^2-Continuity Conditions

$$\mathbf{A} = \Delta\theta \begin{bmatrix} 2 & 1 & 0 & 0 & \cdots & 0 & 0 \\ 1 & 4 & 1 & 0 & \cdots & 0 & 0 \\ 0 & 1 & 4 & 1 & \cdots & 0 & 0 \\ \vdots & \vdots & \ddots & \ddots & \ddots & \vdots & \vdots \\ 0 & 0 & \cdots & 1 & 4 & 1 & 0 \\ 0 & 0 & 0 & \cdots & 1 & 4 & 1 \\ 0 & 0 & 0 & \cdots & 0 & 1 & 2 \end{bmatrix}, \quad \mathbf{C} = \frac{1}{\Delta\theta} \begin{bmatrix} c_{11} & 1 & 0 & 0 & \cdots & 0 & 0 \\ 1 & -2 & 1 & 0 & \cdots & 0 & 0 \\ 0 & 1 & -2 & 1 & \cdots & 0 & 0 \\ \vdots & \vdots & \ddots & \ddots & \ddots & \vdots & \vdots \\ 0 & 0 & \cdots & 1 & -2 & 1 & 0 \\ 0 & 0 & 0 & \cdots & 1 & -2 & 1 \\ 0 & 0 & 0 & \cdots & 0 & 1 & c_{n''n''} \end{bmatrix} \tag{1}$$

in which $n'' = n + 2$, $c_{11} = -1 - \Delta\theta/\tan(\gamma_0)$ and $c_{n''n''} = -1 - \Delta\theta/\tan(\gamma_{n+1})$.

$$\mathbf{P} = \Delta\theta \begin{bmatrix} \frac{1}{\Delta\theta} & 0 & 0 & 0 & \cdots & 0 & 0 \\ 1 & 4 & 1 & 0 & \cdots & 0 & 0 \\ 0 & 1 & 4 & 1 & \cdots & 0 & 0 \\ \vdots & \vdots & \ddots & \ddots & \ddots & \vdots & \vdots \\ 0 & 0 & \cdots & 1 & 4 & 1 & 0 \\ 0 & 0 & 0 & \cdots & 1 & 4 & 1 \\ 0 & 0 & 0 & \cdots & 0 & 0 & \frac{1}{\Delta\theta} \end{bmatrix},$$

$$\mathbf{Q} = \frac{1}{\Delta\theta} \begin{bmatrix} \frac{1}{\tan(\gamma_0)} & 0 & 0 & 0 & \cdots & 0 & 0 \\ -3 & 0 & 3 & 0 & \cdots & 0 & 0 \\ 0 & -3 & 0 & 3 & \cdots & 0 & 0 \\ \vdots & \vdots & \ddots & \ddots & \ddots & \vdots & \vdots \\ 0 & 0 & \cdots & -3 & 0 & 3 & 0 \\ 0 & 0 & 0 & \cdots & -3 & 0 & 3 \\ 0 & 0 & 0 & \cdots & 0 & 0 & \frac{1}{\tan(\gamma_{n+1})} \end{bmatrix} \quad (2)$$

References

[1] Jelaska, D., 2012. *Gears and Gear Drives.* John Wiley & Sons Ltd.

[2] Spitas, V., Costopoulos, T., and Spitas, C., 2005. "Increasing the strength of standard involute geat teeth with novel circular root fillet design". *American Journal of Applied Sciences,* ***2***(6), pp. 1058–1064.

[3] Tiwari, S. K., and Joshi, U. K., 2012. "Stress analysis of mating involute spur gear tooth". *International Journal of Engineering Research & Technology,* ***1***(9), pp. 1–11.

[4] Zou, T., Shaker, M., Angeles, J., and Morozov, A., 2014. "Optimization of tooth root profile of spur gears for maximum load-carrying capacity". *Proc. ASME Design Egineering Technical Conferences, Buffalo, NY, Aug. 17-20, CD-ROM DETC2014-34568.*

[5] Kawalec, A., Wiktor, J., and Ceglarek, D., 2005. "Comparative analysis of tooth-root strength using iso and agma standards in spur and helical gears with fem-based verification". *ASME J. Mechanical Design,* ***128***(5), pp. 1141–1158.

[6] Pedrero, J. I., Vallejo, I. I., and Pleguezuelos, M., 2006. "Calculation of tooth bending strength and surface durability of high transverse contact ratio spur and helical gear drives". *ASME J. Mechanical Design,* ***129***(1), pp. 69–74.

[7] Al-Daccak, M. J., Angeles, J., and A., G.-P. M., 1994. "The modelling of bevel gears using the exact spherical involute". *ASME J. Mechanical Design,* ***116***, pp. 364–368.

[8] Seireg, A. A., and Rodriguez, J., 1997. *Optimizing the Shapes of Mechanical Elements and Structures.* Marcel Dekker, Inc., New York.

[9] Schmit, L. A., 1960. "Structural synthesis by systematic synthesis". *Proc. Second Conference on Electronic Computation ASCE, New York*, pp. 105–122.

[10] Clough, R. W., 1960. "The finite element in plane stress analysis". *Proceedings of the Second ASCE Conference on Electric Computation, Pittsburgh, PA., September.*

[11] Teng, C.-P. "Structural optimization under variable loading conditions". PhD thesis, McGill Univeristy.

[12] Armand, J. L., 1974. "Numerical solutions in the optimization of structural elements". *First International Conference on Computing Methods in Non-linear Mechanics, TICOM, Austin.*

[13] Gallagher, R., and Zienkiewicz, O. C., 1973. *Optimum Structural Design.* John Wiley & Sons, Inc., New York.

[14] Venkayya, V. B., 1971. "Design of optimum structures". *J. Computers and Structures,* ***1***, pp. 263–309.

[15] Mroz, Z., and Garstecki, A., 1976. "Optimal design of structures with unspecified loading distribution". *J. Optimization Theory and Applications,* ***20(3)***, pp. 359–380.

[16] Francavilla, A., Ramakrishnan, C. V., and Zienkiewicz, O. C., 1975. "Optimization of shape to minimize stress concentration". *J. Strain Analysis,* ***10(2)***, pp. 62–70.

[17] Oda, J., 1977. "On a technique to obtain an optimum strength shape by the finite element method". *Bulletin of the JSME,* ***20(140)***, pp. 160–167.

[18] Esping, B. J. D., 1985. "A cad approach to the minimum weight design problem". *International Journal of Numerical Methods in Engineering,* ***21***, pp. 1049–1066.

[19] Angeles, J., 1983. "Synthesis of plane curves with prescribed local geometric properties using periodic splines". *J. Computer-Aided Design,* ***15(3)***, pp. 147–155.

[20] Bidault, F., Teng, C., and Angeles, J., 2001. "Structural optimization of a spherical parrallel manipulator using a two-level approach". *Proc. ASME Design Egineering Technical Conferences, Pittsburgh, PA, Sept. 9-12, CD-ROM DETC2001/DAC-21030.*

[21] Javid, F., Angeles, J., Pasini, D., and Cecere, R., 2012. "Shape optimization of a self-deployable anchor designed for percutaneous mitral valve repair". *ASME J. Medical Devices,* ***6***.

[22] Pehan, S., Kramberger, J., Flasker, J., and Zafosnik, B., 2008. "Investigation of crack propagation scatter in gear tooth's root". *J. Engineering Fracture Mechanics,* ***75***, pp. 1266–1283.

[23] Andrews, J. D., and Hearn, E. J., 1987. "An automatic design optimization procedure to minimize fillet bending stresses in involute spur gears". *International Journal for Numerical Methods in Engineering,* ***24***, pp. 975–991.

[24] Kapelevich, A. L., and Shekhtman, Y. V., 2002. "Direct gear design for spur and helical involute gears". *Gear Technology,* ***September/October***, pp. 29–35.

[25] Spitas, V. A., Costopoulos, T. N., and Spitas, C. A., 2006. "Optimum gear tooth geometry for minimum fillet stresses using bem and experimental verification with photoelasticity". *ASME J. Mechanical Design,* ***128***, pp. 1159–1164.

[26] Bian, X., Fang, Z., Qin, K., Lian, L., and Zhang, B., 2013. "Multi-objective topology optimization for bevel gear and geometrical reconstruction". *J. Applied Mechanics and Materials,* ***278-280***, pp. 139–142.

[27] Kapelevich, A. L., and Shekhtman, Y. V., 2003. "Direct gear design: Bending stress minimization". *Gear Technology,* ***September/October***, pp. 44–47.

[28] Xiao, H., Zu, W., and Zaton, W., 2005. "Fillet shape optimization for gear teeth". *Proc. ASME Design Egineering Technical Conferences, Long Beach, CA, Sept. 24-28, CD-ROM DETC2005-84657.*

[29] Teng, C. P., Bai, S., and Angeles, J., 2008. "Shape synthesis in mechanical design". *Acta Polytechnica,* ***47(6)***, pp. 56–62.

[30] Ristic, D., 2009. "Numberical stress concentration analysis of a driven gear tooth root with two fillet radius". *Scinetific Techincal Review,* ***LIX(1)***, pp. 78–86.

[31] Xie, F., Wang, J., and Wang, Y., 2012. "Finite element analysis of impact of root fillet on bending stress for helical gear of automotive transmission". *J. Applied Mechanics and Materials,* ***184-185***, pp. 214–217.

[32] Flodin, A., and Andersson, M., 2012. “Tooth root optimization of powder metal gears: reducing stress from bending and transient loads”. *Proc. of Powder Metal World Congress and Exhibition (PM2012), Yokohama, Japan*.

[33] Shigley, J., M. C., and Budynas, R., 2004. *Mechanical Engineering Design*, seventh ed. McGraw-Hill Companies, Inc.

[34] Litvin, F., and Fuentes, A., 2004. *Gear Geometry and Applied Theory*, second ed. Cambridge University Press.

[35] Lee, H. W., Lee, K. O., and Chung, D. H., 2010. “A kinematic investigation of a spherical involute bevel-geared system”. *Proc. IMechE Part C, J. Mechanical Engineering Science, DOI:10.1243/09544062JMES1624*.

[36] Park, N., and Lee, H., 2011. “The spherical involute bevel gear: its geometry, kinematic behaviour and standardization”. *Journal of Mechanical Science and Technology,* ***25***(4), pp. 1023–1034.

[37] Figliolini, G., and Angeles, J., 2005. “Algorithms for involute and octoidal bevel-gear generation”. *ASME J. Mechanical Design,* ***127***, pp. 664–672.

[38] Dooner, D. B., 2012. *Kinematic Geometry of Gearing*, second ed. John Wiley & Sons Ltd.

[39] Späth, H., 1995. *One Dimensional Spline Interpolation Algorithms*. A. K. Peters Ltd., Wellesley, MA.

[40] Teng, C. P., and Angeles, J., 2001. “A sequential-quadratic-programming algorithm using orthogonal decomposition with gerschgorin stabilization”. *ASME J. Mech. Design,* ***123***(4), pp. 501–509.

[41] Sánchez, M. B., Pedrero, J. I., and Pleguezuelos, M., 2013. “Critical stress and load conditions for bending calculations of involute spur and helical gears”. *International J. of Fatigue,* ***48***, pp. 28–38.